A vulnerability driven approach to identify adverse climate and land use change combinations for critical hydrologic indicator thresholds – Application to a watershed in Pennsylvania, USA

R. Singh[1], T. Wagener[2], R. Crane[3], M.E. Mann[4], and L. Ning[5]

[1*]Corresponding author. Earth and Environmental Systems Institute, 217F EES Building, Pennsylvania State University, University Park, PA, USA 16802 email: rus197@psu.edu

[2]Department of Civil Engineering, University of Bristol, Bristol, UK

[3]Department of Geography, Pennsylvania State University, University Park, Pennsylvania, USA

[4]Department of Meteorology, Pennsylvania State University, University Park, Pennsylvania, USA

[5]Northeast Climate Science Center, Department of Geosciences, University of Massachusetts-Amherst, Amherst, MA, USA

Key Points

- Method provides valuable information to decision maker in large uncertainties
- Stakeholders define critical thresholds for hydrologic indicators of interest
- We identify land use and climate change combinations that cause vulnerability

Keywords: Decision-making, uncertainty, stakeholder, thresholds, climate change, land use change

* Former- Department of Civil and Environmental Engineering, The Pennsylvania State University, University Park, A, USA

Abstract

Large uncertainties in streamflow projections derived from downscaled climate projections of precipitation and temperature can render such simulations of limited value for decision making in the context of water resources management. New approaches are being sought to provide decision makers with robust information in the face of such large uncertainties. We present an alternative approach that starts with the stakeholder's definition of vulnerable ranges for relevant hydrologic indicators. Then, the modeled system is analyzed to assess under what conditions these thresholds are exceeded. The space of possible climates and land use combinations for a watershed is explored to isolate sub-spaces that lead to vulnerability, while considering model parameter uncertainty in the analysis. We implement this concept using classification and regression trees (CART) that separate the input space of climate and land use change into those combinations that lead to vulnerability and those that do not. We test our method in a Pennsylvania watershed for nine ecological and water resources related streamflow indicators for which an increase in temperature between 3°C to 6 °C and change in precipitation between -17% and 19% is projected. Our approach provides several new insights, for example we show that even small decreases in precipitation (~5%) combined with temperature increases greater than 2.5ºC can push the mean annual runoff into a slightly vulnerable regime. Using this impact and stakeholder driven strategy, we explore the decision-relevant space more fully and provide information to the decision maker even if climate change projections are ambiguous.

Index terms: (hydrology) - modeling, human impacts, climate impacts, (policy sciences) - decision making under uncertainty, (informatics) - data mining

1 Introduction

Freshwater availability is essential for maintaining both the ecological and economic health of a region. We need reliable projections of future streamflow under changing environmental conditions to guide long-term water resources management and planning [*Milly et al.*, 2002, 2008; *Wagener et al.*, 2010]. The information about future streamflow is required at the scale of regional planning [*Barron*, 2009]. However, obtaining this information can be difficult due to large uncertainties in regional estimates of climate change projections [*Hall*, 2007; *Beven*, 2011; *Collins et al.,* 2012].

Common methods to estimate the impact of climate change on water resources include direct use of climate model output or the linking of general circulation models (GCMs) to hydrologic models via downscaling [*Xu et al.*, 2005]. The latter is the most widely used strategy to obtain projections of hydrologic variables. Literature is abundant with studies that use downscaled GCM outputs as forcing for a hydrologic model to derive projected hydrologic changes in a region [e.g. *Maurer and Duffy*, 2005; *Kay et al.*, 2009; *Manning et al.*, 2009; *Teng et al.*, 2012; *Bennett et al.*, 2012]. In this study, we will call this modeling chain from GCMs to hydrologic models the hydro-climatic framework (Fig. 1a).

There are several challenges in using this hydro-climatic framework for estimating future streamflow. First, there are large uncertainties in the streamflow output from the hydro-climatic framework that stem from a range of sources [*Paton et al.*, 2013]. To begin with, there is uncertainty due to the chosen emission scenario. The further we project into the future, the more the projections from different emission scenarios separate. Secondly, GCM projections have large uncertainties (depending upon the region) mainly due to parameterization of cloud physics, uncertainty in climate sensitivity etc. The overlap in the underlying physics in these models limits our ability to construct an ensemble of climate models that can reasonably estimate the probability distribution of climate projections, since they do not represent independent samples [*Stephenson et al.*, 2012; *Knutti et al.*, 2013]. There are also significant uncertainties in the hydrologic model, including model structural uncertainty and a dependence of the model parameters on the climate in the calibration period [*Merz et al.*, 2010; *Singh et al.*, 2011, 2013]. A priori parameters can be used instead, but generally exhibit large uncertainties if these are estimated [*Kapangaziwiri et al.,* 2012]. Hence, the traditional forward propagation approach that integrates uncertainty from different sources may lead to biased or over-confident hydrologic projections that might be ineffective in aiding decision makers [*Hall*, 2007; *Beven*, 2011].

So, while we generally assume that significant amount of uncertainties are present, we do not know the actual amount and we often lack the ability to attribute the total estimated uncertainty to its sources (e.g. choice of GCM, downscaling, GCM parameters etc.). The contribution of different sources of uncertainty to the total uncertainty in streamflow projections depends on the study region, the hydrologic indicator considered, the hydrologic model used etc [*Chen et al.*, 2011; *Dobler et al.*, 2012; *Teng et al.*, 2012; *Bosshard et al.*, 2013]. For example, *Teng et al.* [2012] find that streamflow projections are more uncertain for drier regions within their study area in southeastern Australia. They also find that uncertainties in projections of low flow characteristics are higher for regions that are likely to experience large declines in future rainfall. *Chen et al.* [2011] also show that the relative contribution of uncertainty from different sources varies with the hydrologic metric being evaluated. *Dobler et al.* [2012] show that even though GCM uncertainties dominate hydrologic projections for most of the year, the uncertainty from hydrologic model parameters is greater than uncertainty from GCMs during some winter months. These recent findings also challenge the conclusions from earlier studies that the uncertainty arising from GCMs or downscaling methods often overshadows those originating from the choice of hydrologic model structure or hydrologic model parameters [*Wilby and Harris*, 2006; *Kay et al.*, 2009; *Prudhoome and Davies*, 2009a&b]. While traditional forward propagation approaches (Fig. 1a) may be used to gain understanding of possible changes in streamflow, decision makers do not always find this information helpful given that they can often include projections that suggest both positive and negative changes in streamflow (mainly due to precipitation). Recent studies have proposed alternative bottom-up or vulnerability based approaches for dealing with problems such as water management decisions under large projection uncertainties [*Lempert et al.*, 2008; *Wilby and Dessai*, 2010; *Brown et al.*, 2011; *Weaver et al.*, 2013]. In essence, these alternative paradigms invert the problem by following a 'bottom-up' approach as shown in Figure 1(b). Here, stakeholders define vulnerability ranges for a particular decision variable, e.g. a specific hydrologic indicator, from the outset. Then, all combinations of climatic input and model parameters that cause the variable of interest to transition into vulnerable regimes are identified through a modeling framework. Finally, the available information on future climate is integrated to assess the plausibility of the hydrologic indicator to transition into a vulnerable regime in the future.

These bottom-up approaches are sometimes also termed decision scaling or context-first approaches. They can be used in a wide variety of problems and have proved very useful for decision-making when projections of the future are highly uncertain [*Moody and Brown*, 2013; *Kunreuther et al.*, 2013]. *Lempert et al*. [2008] describe two possible methods to identify vulnerable regions in the input space – patient rule induction method (PRIM) and classification and regression trees (CART). Neither of these methods is found to be significantly superior to the other in *Lempert et al.* [2008]. However, PRIM is generally employed when the output space is partitioned in two possibilities – vulnerable or non-vulnerable. Other example applications of these alternative approaches include risk-based decision making to characterize contaminant plumes by *Boso et al.* [2013], and the use of decision tree models for estimating the value of information provided by a groundwater quality monitoring network by *Khader et al.* [2013].

In this study, we present a method based on this bottom-up paradigm that provides decision makers with information about adverse thresholds in climate and land use change that may cause a hydrologic indicator to transition to vulnerable regimes. These thresholds can directly be used to inform policy decisions even if uncertainties in future climate projections are large. For example, if an indicator quickly transitions into vulnerable regimes (small changes in climate or land use causing vulnerability - low thresholds), it provides the decision maker with the foresight that a very robust policy or drastic actions will be needed to avoid potentially large damages. In this way, the information about thresholds in climate or land use obtained can be combined with the available information on projected climate change (with small or large range of uncertainties) to provide the decision maker with better insights into the nature of the hydrologic indicator, its dominant controls, possible tipping points, feasibility of crossing those tipping points, etc.

The objective of our study is to implement and test a classification tree method centered on a vulnerability-based approach for change assessment. We test our approach in the Lower Juniata watershed in Pennsylvania located in the northeastern USA for nine different hydrologic (streamflow) indicators. We derive classification trees for these indicators using a large range of possible climates, land uses and hydrologic model parameters. The large range of climates is generated by applying the delta change method to precipitation and temperature time series to the historical period of 1948-1958. A vegetation parameter in the hydrologic model approximates the land use and uncertainty in the ranges for other hydrologic model parameters is based on their a priori values derived from the watershed physical characteristics.

Using these classification trees, we demonstrate how our proposed method provides additional information to a decision maker as compared to the standard approach by generating estimates of critical thresholds in climate as well as an understanding of relative importance of climate and land use change within the hydrologic modeling framework. For example, the available downscaled projections of climate from nine general circulation models (GCMs) for the baseline (1990-2000) and end of century (2090-2100) time periods are used to navigate the classification tree to arrive at the future values of the indicators (eg. mean annual runoff) and assess the impact of changing climate on the hydrologic indicator. We then compare the projections from the classification tree based approach to those from the standard approach by driving a historically calibrated hydrologic model using future projections of downscaled climate.

2 Methodology, model and data

2.1 A classification tree based strategy for identifying critical climate and land use change combinations

The main goal of our study is to establish the relationship between different possible climate and land-use changes in our study watershed and resulting streamflow indicator values (Fig. 2). To achieve this goal, we invert the problem through exploratory modeling. We start by defining a feasible space of climate and land use changes. Land use is represented as a parameter representing the fraction of deep-rooted vegetation in the watershed – assuming that this is main aspect of vegetation that matters for the hydrologic indicators studied here. Other processes and land use characteristics can be easily included. Different feasible climates are generated using the delta change method in which only the mean of the climate variables (precipitation and temperature) is changed keeping the higher moments fixed [*Nash and Gleick*, 1991; *Jones et al.* 2006]. Following this definition of the feasible input space, we establish different classes for the hydrologic indicator of interest. Here the stakeholder would normally be asked to provide their definition of vulnerable ranges of streamflow indicators. This could for example be an ecologist who defines critical values for a particular aquatic species, or a water resources manager who has to fulfill multiple competing demands throughout the year.

In our study, we establish the following grouping to demonstrate the methodology: if the value of the selected indicator is within historical variability, it falls in Class 1, if it is only slightly above historically observed values, it is assigned Class 2, and extreme increases are grouped in Class 6. We develop similar classes for values that are below the observed historical variability. Each resultant value of the hydrologic indicator obtained from a particular combination of climate and land use can then be assigned a class based on these class definitions. Even though we start with a possible classification of hydrologic indicator space to demonstrate the method, stakeholders can adjust this approach by defining their own vulnerability classes and identify how climate or land use change will impact the indicators that most interest them. This will allow them to have an understanding of not just the specific projections of streamflow based on climate model outputs but the general behavior of their indicator. Using the mapping from input climate and land use space to output indicator space, they can decide how robust the policy for dealing with future changes should be.

Using N climates and P parameter combinations, we derive NxP values of hydrologic indicators of interest by driving the hydrologic model with these combinations and assign them to their specific class. Next, we use the classification and regression tree (CART) to relate the climate and land use changes to the different classes of the streamflow indicator. CART is a binary recursive partitioning algorithm that divides the input space of multiple variables into sub-spaces, with each sub space related to a particular class of output variable [*Breiman et al.*, 1984]. At each stage, the tree partitions the space based on maximum gain in information. Thus, through CART analysis, we can assess the critical changes in land use and climate required to push the streamflow indicators into different regimes (represented by the indicator classes). Once we obtain the information regarding the critical combinations in climate and land use, we can include the available downscaled climate data into the analysis. Using the future projections of climate change derived from downscaled GCMs, we can assess the plausibility of the hydrologic indicator to transition into a vulnerable regime. Similarly, we could assess specific land use change scenarios for the study region.

2.2 Hydrologic Model

Figure 3 shows the hydrologic model structure used in this study adapted from the top-down modeling framework by *Bai et al.*, [2009] and *Farmer et al.* [2003]. The model has a spatially-lumped parsimonious model structure and is run at a daily time step. It comprises of a snow module followed by a soil moisture accounting module and a routing module. There is possibility for recharge from the saturated soil store to the deeper groundwater store. The soil moisture accounting module splits the soil into two layers – unsaturated and saturated stores. The soil depth is modeled using a multiple bucket scheme based on the ten-bucket Xinanjiang-model distribution [*Zhao et al.*, 1980; *Son and Sivapalan*, 2007; *Bai et al.*, 2009]. The multiple buckets are filled and spilled in a parallel configuration.

Evapotranspiration is estimated by dividing the catchment surface into bare soil and deep-rooted vegetation covered areas. The soil profile is divided into unsaturated and saturated zones. ET from the saturated zone is proportional to potential evaporation and the soil moisture content. The saturated zone ET is modeled similarly for both bare soil and vegetation covered fractions. The main difference in ET arises within the unsaturated soil store. In the unsaturated zone, the fraction of the watershed covered by bare soils evaporates at a rate that is proportional to the soil water content and to the potential evaporation. While in the case of vegetation-covered soils, transpiration from the unsaturated stores is controlled by field capacity parameter. If the soil moisture content exceeds field capacity, transpiration occurs at potential rate. The basic formulation is adapted from *Bai et al.* [2009], with modifications for including phenology and leaf area index from *Sawicz et al.* [2013]. Equations are included in the Appendix A.

The growing behavior of vegetation, efficiency of water extraction from the soil, and variable canopy interception are included in the model to represent phenology in three ways. Above 10°C, water extraction by vegetation is considered unimpeded and is set at its maximum capacity. Below -5°C, water extraction efficiency is considered to have stopped so there is no evapotranspiration. Between these two ranges, a linear relationship between extraction efficiency and temperature is assumed. The canopy interception is modeled as maximum canopy interception during summer months and a minimum during winter months. A sinusoidal function is used to describe the canopy interception for periods between summer and winter. Details of model equations are provided in Appendix A and Table 2 lists the feasible range of parameters based on literature review.

2.3 Study area – The Lower Juniata Watershed

The Lower Juniata watershed is located in the northeastern United States (Fig. 4). The area of the watershed is around 8686 km^2, which encompasses roughly 12% of the area of the Susquehanna River basin. Most of the watershed is covered by forests (~70%), followed by agriculture (~23%) and urban land use (~7%) [*Falcone et al.*, 2010]. Baseflow index estimated from the hydrograph of the gauge located at the Juniata River at Newport, PA is around 0.70. The baseflow index is estimated using a single pass filter by *Arnold et al.* [1995]. Mean annual precipitation (P) for the period 1948-58 is 1007 mm/year and mean annual potential evapotranspiration (PE) estimated from the Hargreaves equation [*Hargreaves and Samani*, 1985] is around 1066 mm/year resulting in an aridity index of around 1. The mean annual flow (Q) for the period 1948-58 is 444 mm/year resulting in long term runoff ratio (Q/P) of 0.44.

2.4 Data

The historical streamflow, temperature and precipitation data is obtained from the MOPEX dataset [*Duan et al.*, 2006]. The downscaled climate data used in the study is derived using the probabilistic downscaling method by *Ning et al.* [2012a,b]. Table 3 lists the number of global climate models (GCMs) used for this analysis. We also use the data from Falcone database [*Falcone et al.*, 2010] for obtaining watershed properties such as land use, soil types, etc. to derive a-priori ranges of hydrologic model parameters.

2.5 Classification and regression trees

Classification and regression tree (CART) is a recursive partitioning algorithms used to classify the space defined by the input variables (here hydrologic model parameters and climate) based on the output variable (here categorized hydrologic indicators) [*Breiman et al.*, 1984]. In this study, we apply CART analysis using the statistical CART package of R called ‘rpart’ [*Therneau and Atkinson*, 2010]. This method automatically provides a pruned tree after a tenfold cross validation and also provides estimates for the misclassification error rates and cross-validation error rates for the classification trees developed.

The resulting tree consists of a series of nodes, where each node is a logical expression based on the values of a hydrologic model parameter or a climate variable in the input space. If the expression is true, the left branch is followed; otherwise the right branch is followed. In this way, one can follow different combinations of expressions (representing multi-dimensional sub-spaces of the input variables) to arrive at a terminal leaf, which represents the output variable class with the highest probability. Since the classification is imperfect, the CART analysis also provides information on the probabilities of different output classes at each terminal leaf node. The histograms of class distributions at each terminal leaf node visualize these probabilities, thereby providing an assessment of the uncertainty associated with the classification.

3 Results

3.1 Obtaining a-priori ranges for hydrologic model parameters

We include parametric uncertainty in this analysis by obtaining a-priori parameter ranges largely based on physical watershed characteristics. This is achieved in two ways - relating the different components of the hydrologic model with observed physical characteristics of the watershed from the Falcone database and recession curve analysis of the historical streamflow data. Using this approach, a-priori ranges are obtained for seven out of twelve parameters. For the remaining parameters, feasible ranges are obtained from literature [*Farmer et al.*, 2003; *Van Werkhoven et* *al.*, 2008; *Kollat et al.*, 2013]. The a-priori ranges are estimated for two recession parameters, two soil parameters and three vegetation parameters.

We derive a-priori ranges for two parameters related to the soil module - soil depth and field capacity. Soil depth is obtained based on the available depth to bedrock estimates, and porosity estimates of sand, silt and clay (all three are present in the watershed in significant amounts - 50% silt, 30% sand and 20% clay). Field capacity parameter range is estimated as the range of the field capacity parameter across sand, silt and clay using the information on watershed average available water capacity, porosity and permanent wilting point ranges for sand, silt and clay. Vegetation parameter is estimated from land use information about the watershed [*Falcone et al.*, 2010]. The percentage forest cover in the watershed is around 70%, so the range of fraction of deep-rooted vegetation in the watershed is fixed between 0.6-0.8. Leaf area index values are fixed between 0-6, since most the forests are deciduous in nature. Appendix tables B1-B3 lists these calculations in details.

Two recession parameters are present in the model - recession coefficient 1 (A_{ss}) for subsurface flow from the saturated store and recession coefficient 2 (A_{bf}) for baseflow from the ground water reservoir. These are obtained from analyzing the recession behavior of the available streamflow time series. Since the model does not route the surface flow, recession analysis is carried out only on baseflow component of the total streamflow, which is derived from the base flow filter [*Arnold et al.*, 1995]. Two slopes are estimated for each year across a 10-year time period. Recession coefficient 1, which represents the recession from saturated store, is estimated as the average slope across the fast recession limbs (6-14 days). Recession coefficient 2, which represents the recession from the ground water reservoir, is estimated by constructing a master recession curve for the recession after removing the faster recession limbs

(50-83 days). Figures B1-B2 shows the estimation procedure of routing parameters as derived from the streamflow hydrographs and Table 2 lists the ranges.

3.2 Climate scenarios

The delta change method described in Section 2.1 is used to generate climate change scenarios. The historical period of 1948-1958 is used as the base period and changes in temperature and precipitation are applied on the climate time series for this period. The ranges for precipitation change explored are -50% to +50% in steps of 10%. The ranges for temperature change are 0°C to 8 °C in steps of 1°C. Therefore, the total number of climate combinations explored is 99. The adjustments to the climate data were made at daily time steps with the precipitation values multiplied by a suitable fraction between 0.5-1.5 and the temperature values increased by 0-8 °C. To provide an estimate of how wide these ranges are - the IPCC 4th assessment report [*Christensen et al.*, 2007] suggests changes in precipitation between -3% to 15 % and temperature increase between 2.3-5.6°C from 1980-99 to 2080-99 for Eastern US under the A1B emission scenario. It is important to note here that we use two different climate data in the study - the climates generated from the delta change method are used to explore the feasible climate space, whereas, the downscaled climate data by *Ning et al.*, [2012a,b] is used once the (synthetic) climate and land use space has been related to the hydrologic indicator. The synthetic climate data is used to explore the climate space and build the classification trees. The downscaled climate data is used to assess the plausibility of the watershed to transition into a vulnerable regime in section 3.8 once the tree is derived.

3.3 Defining classes for streamflow indicators

In this study, we assume that we want to analyze the major controls on indicators representing aspects of streamflow relevant for ecology as well as water availability for human abstractions such as power generation. Magnitude related indicators such as mean annual runoff would determine average water availability. Seasonal variability of water availability will be represented by indicators related to flow in months of high/low flows. *Olden and Poff* [2003] describe several indicators that are ecologically relevant as well as represent water availability. Based on the insights provided by them, we include 4 categories of indicators in our analysis (Table 1).

- Magnitude related indicators include mean annual runoff, minimum April flow, and maximum August flow. As shown in Figure B3, August is a low flow month for this watershed, and April is a high-flow month. Therefore, flows for both months are included in the analysis.
- Frequency related indicators include low flow pulse count and flood frequency. These are important to assess the recurrence of low/high flow conditions in the watershed, which will be critical for in stream flora and fauna.
- Duration related indicators include low flow pulse duration and high flow pulse duration. Low flow pulse duration is particularly important since it assesses the number of days low flows will sustain in the watershed and is very important to assess water availability for power production during summer months.
- Indicators describing the timing and rate of change of streamflow include seasonal predictability of non-flooding and reversals.

We define classes for each indicator as shown in the example illustrated in Figure 5. These class definitions are fixed across all indicators. The range of indicator values for each class is estimated using the standard deviation calculated from the historical data. A 10-year running window from 1948-2002 is used to estimate 45 values for each indicator. We find that a range of

4σ, where σ is the standard deviation of the indicator values in the running window between 1948-2002, is sufficient to cover all indicator values in most cases. Therefore, the width of each class is fixed at 4σ. The different indicator classes are defined using the mean (μ) and standard deviation (σ) from the historical period as follows:

- Class 1 – Historical range: $\mu-2\sigma < \text{Value} < \mu+2\sigma$
- Class 2 – Slightly higher than historical range $\mu+4\sigma < \text{Value} < \mu+8\sigma$
- Class 3 – Much higher than historical range $\mu+8\sigma < \text{Value} < \mu+12\sigma$
- Class 4 - Slightly lower than historical range $\mu-4\sigma < \text{Value} < \mu-8\sigma$
- Class 5 – Much lower than historical range $\mu-8\sigma < \text{Value} < \mu-12\sigma$
- Class 6 – Extremely high ranges $\mu+12\sigma < \text{Value}$
- Class 7 – Extremely low ranges $\text{Value} < \mu-12\sigma$

If the lower limit of a class is falls below zero, it is set equal to zero and the remaining classes below this limit are eliminated.

3.4 Classification results for changing climate and fixed land use

10000 random parameter sets are generated from the a-priori parameter ranges in Table 2 using Latin Hypercube sampling. Based on the method described in Figure 2, we drive the hydrologic model with 99 climates and 10000 parameter combinations to estimate the value of streamflow indicator for each combination. In this way, we end up with 990,000 values for each indicator across a broad range of climates, land use (represented by the fraction of deep-rooted vegetation parameter) and watershed properties (represented by the range of a-priori parameter sets). After this, we assign each indicator value a class based on whether it falls within the range of historical variability or outside it, as described in section 3.3. Then, classification and regression trees (CART) are used to relate the different classes of indicators (output variable) with input climate and parameter space (input variables). The data on misclassification and cross-validation rates for the classification trees derived in this study are included in Appendix C. Here we will focus our analysis of three selected indicators to show the application of the method, the classification trees for the remaining indicators are included in Appendix C -

- Mean annual runoff – this indicator represents general water availability
- Maximum August flow – August is a month of low flows and this indicator suggests the condition of low flows
- Flood frequency – indicates the condition of high flows

We start with the controls on flood frequency for the case of changing climates but fixed land use. In this case, the fraction of deep-rooted vegetation is fixed at the historical range. Figure 6 (a) shows the different class assignments based on historical variability of flood frequency derived from streamflow data. Class definitions have been provided in Section 3.3. Here we assume that an increase (shown by yellow and shades of red) in the value of the flood frequency will lead to vulnerability since that corresponds to the watershed experiencing high floods more frequently, a decrease is assumed to have uncertain impacts (shown by shades of green).

Figure 6 (b) shows the classification tree for flood frequency for fixed land use but changing climates. The tree consists of many nodes, each of which is a logical expression. If the expression is true, the left branch is followed, otherwise the right one. In this manner, by navigating different sub-spaces of climate and parameters, we reach a 'terminal' node or a leaf. At the leaf, the indicator class that results from the combination of different logical expressions is shown. From the tree in Figure 6 (b), we find that the primary control on this indicator is precipitation (shown as Pratio – the ratio of mean annual precipitation in the future to historical mean annual precipitation) followed by the recession coefficient describing the recession from the subsurface soil moisture store (Ass). The maximum height of soil moisture storage (Sb) is the third control. This suggests that frequency of high floods depends first upon the climate of the watershed followed by its ability to release water from the subsurface and amount of water that can be stored in the subsurface.

We also show the class probabilities associated with the classes 1 to 7. This gives an indication of how 'pure' a terminal node is. If all the indicator values based on navigating a set of logical expressions resulted in a single class, the probability distribution will be skewed towards that class. On the other extreme, if the classification algorithm is unable to relate the indicators class with specific regions in the input variables space, the node will be highly impure, or the probability distribution across classes 1 to 7 will be nearly flat. Most of the times the probability distribution are in the middle of these two extremes suggesting there is always some uncertainty in threshold values of climate and parameters selected by the classification algorithm.

Using Figure 6 (b), one can also identify the different pathways that lead to vulnerability of the indicator as shown by solid black lines. Even for small rises in mean annual precipitation (increase of 5% from historical value) the indicator can transition to different dominant controls. In this case, if the mean annual precipitation is greater than 0.95 times the historical value, the indicator's classes are controlled by the recession coefficient, Ass and maximum height of soil moisture storage, Sb. If not, further changes in mean annual precipitation control the indicator values. Following the left branch of the classification tree, we find that if mean annual precipitation changes remain within 0.95 to 1.15 times the historical value, the most likely values of flood frequency fall into Class 1, i.e., the indicator remains within historical variability. On the other hand as mean annual precipitation rises beyond 1.15 times its historical value, model parameters emerge as significant controls on the classes for the indicator. It is worth pointing out that even though temperature is varied across a wide range in this analysis (0 to 8 °C), it does not show up at all as a dominant control for flood frequency.

We can conclude from this tree that if the watershed witnesses an increase in precipitation, both the amount of increase and other watershed properties will govern the future values for flood frequency. On the other hand, if the watershed transitions into decreasing precipitation regimes, precipitation itself will be the dominating control on this indicator. Using available data on future climate projections and historical streamflow, we can further assess the plausibility of the different paths as discussed in sections 3.7 and 3.8.

Instead of using class widths as 4σ as described in section 3.3, if we use 6σ as the width of each class, the resultant tree is shown in Figure 6 (c). For the flood frequency indicator, if the thresholds are shifted to larger limits, it does not impact the dominant patterns in the classification tree. Precipitation is still the major control and its thresholds remain consistent between Figure 6(b) and Figure 6(c). Similarly recession coefficient Ass also remains an important control and its thresholds are the same between the two classification trees. The changes are found at lower levels of the tree – absence of Sb (maximum height of soil moisture storage), addition of temperature as a control and a slight modification of threshold of Pratio from 0.85 in Figure 6(b) to 0.75 in Figure 6(c). Sine the class widths are defined to be wider in Figure 6(c), larger changes in precipitation are now required to shift the regimes of the hydrologic indicator. As before, even small changes in precipitation (5%) can lead to a shift in dominant controls.

3.5 Combined impact of climate and land use change on streamflow indicators

We estimate the combined impact of climate and land use change by allowing the fraction of deep-rooted vegetation to vary from 0 to 1, representing no forest cover to full forest cover in the watershed. We compare the case of fixed and varying land use for 2 indicators - maximum august flows and mean annual flows as shown in Figure 7. The left panel in the Fig. 7 shows the classification tree for changing climate and fixed land use, the right panel shows the classification trees for varying both climate and land use in the watershed. The impact of changing land use varies across the two indicators – mean annual runoff in Fig. 7a and maximum august flow in Fig. 7b. Several interesting patterns are discovered -

I. Type I impact – A decrease in fraction of deep-rooted vegetation cover increases the odds for the mean annual runoff to transition to higher values (Figure 7a). Also, once the fraction of deep-rooted vegetation is allowed to vary from 0 to 1, land use becomes the 2nd most dominant control on mean annual runoff. However, if the fraction of deep-rooted vegetation is fixed in the historical range, temperature is the 2nd most dominant control. In general, we find that a small deep-rooted vegetation cover corresponds to high values of mean annual flow. For example, Figure 7 (a – right panel) shows that for a 25% increase in mean annual precipitation, the mean annual runoff always belongs to class C3 when the percentage deep-rooted vegetation less than 36%. But when this percentage is allowed to be greater than 36%, the indicator can belong either to Class 1 or in Class 2 based on the values of temperature and climate change.

Our results agree with *Frans et al.* [2013] who show a 5% increase in runoff when forests (deep-rooted vegetation) are replaced by croplands (shallow rooted) in the upper Mississippi river basin. Similarly, we find that a decrease in percentage of deep-rooted vegetation leads to a higher chances of the mean annual runoff belonging to class 3.

Another way of interpreting this result is that for a given climatic regime in a watershed, the input precipitation (P) is partitioned into green (ET) and blue water (Q) on the basis of extent of deep-rooted vegetation cover. So an increase in one will logically lead to a decrease in other.

II. Type II impact – A high fraction of deep-rooted vegetation cover is the only way some indicators can maintain their historically observed ranges. Maximum August flows would be much higher (belonging to classes 2, or class 5) than its historically observed range (Class 1) if the percentage of deep-rooted vegetation in the watershed decreased beyond 32% (Figure 7b – right panel).

III. Type III impact – Deep-rooted vegetation cover interacts with climate to generate different possible states for the watershed. For example, keeping the percentage of deep-rooted vegetation in the watershed above 43% may prevent extreme increases in maximum August flows. If the vegetation falls below 44% the maximum August flows will always belong to class 5 (Figure 7b – right panel). The classification trees for combined climate and land use change show how these two type of changes interact with each other to generate different regimes for a hydrologic indicator.

In general, we find that until deep-rooted vegetation in the watershed falls below 50%, it will not become a major factor on controlling the different hydrologic indicators since the split values in logical expressions for fraction of deep-rooted vegetation picked by CART is less than 50% in almost all cases. On the other hand, even small changes in precipitation (~5%) significantly impact the dominant controls on the indicator. For the classification trees showing the impact of deep-rooted vegetation for other hydrologic indicators, see Appendix C, Figures C1-C6.

3.6 Dominant controls for all hydrologic indicators

Figure 8 summarizes the different controls on the nine hydrologic indicators analyzed in this study. We assess the importance of different controls for each indicator by using its classification tree. The input variable (climate or hydrologic model parameter) that forms the first split in the tree is assigned maximum importance because among all input variables it is the one that can classify the output space most effectively (maximum gain in information). In this manner, based on the location of different input variables in the tree, we assign them a relative importance. This assignment is depicted by different shades of gray and is shown in the legend in Figure 8. We show these controls for three cases – when parameters vary across their entire feasible range, parameters are fixed at their a-priori ranges, all parameters except the fraction of deep-rooted vegetation cover are fixed at their a-priori ranges (the case of varying land use).

We observe that the controls vary across indicators. Across the entire feasible ranges of parameters, for magnitude related indicators, climate is the primary control, soil parameters are the secondary control and vegetation together with recession (or routing) parameters are tertiary controls. The recession parameters are not important at all for two out of three magnitude related indicators. For flood frequency, climate and soil parameters are dominant, whereas, recession parameters are most important for low flow pulse count. For low flow pulse duration, precipitation is the dominant control followed by soil, vegetation and recession parameters. On the other hand, high flow pulse duration is mainly governed by the recession parameters; climate has a secondary effect and vegetation with soil parameters have a tertiary effect. For rate of change indicator (reversals), soil parameters are the important controls followed by vegetation and climate. No statistically significant trees are obtained for seasonal predictability of non flooding in the case of feasible parameter ranges.

When we reduce the feasible space to a-priori ranges of hydrologic model parameters based on watershed physical properties, temperature shows up as an important secondary control for two out of three magnitude related indicators. For magnitude related indicators, climate is the dominant control with both precipitation and temperature being present in the classification tree. For monthly flows (minimum April and maximum August), soil parameters also have tertiary importance. For low flow pulse count, climate and soil parameters (deep recharge coefficient and soil shape parameter) are important. For flood frequency, climate is the primary control (also seen in detail in Figure 6) followed by recession and soil parameters. For duration related indicators too, climate followed by recession and soil parameters are the main controls. The controls for rate of change (reversal) are similar as the case of feasible space with climate becoming the most important in restricted parameter space. The predictability of non-flooding is governed mainly by soil parameters followed by climate. However, this tree has a very skewed distribution with most of the indicator values belonging to the historical class (root node in Figure C5) and therefore the classification is not reliable. Once we allow the fraction of deep-rooted vegetation in the watershed to vary from 0 to 1 (the case of changing percentage vegetation), land use turns out to be the secondary control across all indicators. It is particularly important for low flow pulse count, low flow pulse duration, timing and rate related indicators.

3.7 Impact of parametric uncertainty when navigating the classification trees

In order to ascertain which path in a classification tree the watershed will follow, we need estimates of model parameters. Figure 9a shows classification tree for flood frequency (section 3.4 and Figure 6) based on a range of climates, fraction of deep-rooted vegetation fixed at historical ranges, and a-priori ranges of parameters. A further reduced range of values for important parameters selected on the basis of calibration are shown in Fig. 9b. Out of 10000 parameter sets generated using uniform random sampling, 19 parameter sets satisfying Nash-Sutcliffe Efficiency (N.S.E) >0.75 on Box-Cox transformed flows (using a Box-Cox parameter value of 0.3) and absolute bias error <10% are chosen to represent the range of parametric uncertainty [*Nash and Sutcliffe*, 1970; *Brazil*, 1988; *Kottegoda and Rosso*, 1997]. The Nash-Sutcliffe Efficiency was estimated for daily time steps and the absolute bias error was estimated as the difference between total runoff simulated and observed across the 10-year period.

Even across a relatively small set of high performing parameter sets, the ranges of parameters are high. High parametric uncertainty blurs the differentiation between the plausibility of different paths. We find that high uncertainty in recession coefficient, Ass, leads to two paths being feasible while analyzing the region of space with increases in precipitation beyond 15% of the historical value. This indicates the need for reducing these uncertainties in order to decrease the range of possible futures. The tree also demonstrates how uncertainties in climate and parameters interact with each other in a complex manner. Even if we know for certain the future climate, existing parameter uncertainties makes the projection of future regime of indicator uncertain.

We generally do not observe such an impact of hydrologic model parameters on estimates of hydrologic indicators in other studies since they focus mainly on magnitude related indicators. In this study too, the magnitude related indicators (such as mean annual runoff), are mainly dependent on the climate of the watershed (Figure 8, the case of a-priori parameter ranges). Even when studies explore different indicators they only vary the analysis between high and low flow magnitude indicators. But if we move beyond magnitude related indicators towards frequency and duration related indicators, the hydrologic model parameter uncertainty becomes much more important as seen in the example provided in Figure 9.

3.8 Comparing top-down with bottom-up approach

Finally, we compare the traditional top-down approach for deriving streamflow projections to the bottom-up approach used in this study. We derive the future values for different indicators using projections of future climate based on a statistically downscaled ensemble. We obtained future climate information from 9 GCMs (Table 3) and 1500 realizations per GCM based on the method in *Ning et al.*, [2012 a,b]. We use 19 parameter sets that satisfy a bias error < 10% and N.S.E >0.75 on Box-Cox transformed flows. This represents the classical calibration based approach. Figure 10a shows the ranges for change in precipitation and temperature based on downscaled climate data, 10b shows the classification tree for mean annual runoff derived from climates generated by delta-change method, and 10c shows the future projections of streamflow obtained by the tradition top-down approach. By using the range of future precipitation and temperature change from downscaled climate data in Fig. 10a, we can assess projected future streamflow from the classification tree in Fig. 10b by following the branches of the tree that represent temperature change between 3 °C and 6 °C and precipitation change between 0.83 to 1.19 times the historical mean annual precipitation. On comparing the projections of streamflow in Fig. 10c with those from the CART analysis in Fig. 10b, we find that both analyses project future mean annual runoff to be either within the historical range or to decrease (Class 4). However, CART analysis provides additional information about the thresholds in climate, which the traditional top-down approach does not. For example, following the left most branch of the tree in Fig. 10b, we find that a temperature change greater than 2.5°C will keep the future streamflow within the historical range (Class C1) even if precipitation increases between 25% and 35%.

We can also visualize all the combinations of input climate and parameters that lead to a particular class of hydrologic indicator using high dimensional data visualization. An example for mean annual runoff is shown in Figure 11. The results are plotted as parallel co-ordinate plots with the normalized values for all parameters and climate change ranges. The temperature increase is normalized between 0°C to 8°C, and the precipitation change is normalized between 0.5 and 1.5 times the historical precipitation. Other parameters are normalized according to a-priori ranges of model parameters.

Figure 11 shows that only precipitation and temperature are the main controls on mean annual runoff, with precipitation being primary and temperature being a secondary control. We find that only low values of temperature increases can lead to mean annual runoff transitioning to Class 3 as seen from the skewed distribution in temperature change for the subplot showing Class 3 (green). Note that the classification tree does not provide much information about the climate combinations that lead to Class 3 - there is no node in Figure 10(b) that results in C3. Visualization such as those in Figure 11 can be further used to explore such classes that do not emerge as prominently in the classification tree. Figure 11 suggests that if the temperature increases beyond 2°C to 3°C, no matter how high the precipitation increase will be, streamflow is not likely to be as high as the ranges in Class 3. On the other hand, large decreases in precipitation always result in extremely low streamflow values (C5) despite constant or increasing temperature. Therefore, we find that the sensitivity of streamflow to temperature changes is a function of precipitation change. Streamflow is very sensitive to temperature change when precipitation increases by amounts [25%-35%] and relatively insensitive to temperature change if precipitation decreases beyond -35% of the historical value.

4 Discussion

We find that critical thresholds for climate and land use change vary across indicators. For example, small decreases in precipitation (~ -5%) combined with temperature increases greater than 2.5°C can cause mean annual runoff to transition into a slightly vulnerable regime. The mean annual runoff remains within historical variability when either the precipitation change remains between -5% to 15% and temperature increases are less than 2.5°C, or temperature increases beyond 2.5°C and precipitation increases between 25% to 35%. Even for other frequency/duration indicators like low flow pulse duration, small decreases in mean annual precipitation (>5%) can shift its values outside historical variability (Figure C3).

We also find interesting interactions between climate and land use change in the watershed. Deep-rooted vegetation cover plays a dual role in the hydrology of a watershed – it makes low flow conditions more severe due to larger evapotranspiration, but also mediates the impacts of high flows. For example, the classification tree showing the controls on low flow pulse duration with varying fraction of deep-rooted vegetation (Figure C3, lower panel) illustrates that for all cases of mean annual precipitation decreases between -35% to -15% of the historical value, and percentages of deep-rooted vegetation less than 36%, the indicator has high probability of belonging to the slightly vulnerable class – Class C2. But for the same range of mean annual precipitation, if the percentage of deep-rooted vegetation is greater than 36%, the indicator has higher chances of belonging to much higher vulnerability classes – C3 and C6. So an increase in percentage of deep-rooted vegetation leads to increased chances of persistence of low flow conditions in the stream. This is similar to a recent observation from four headwater catchments in central and Western Europe by *Teuling et al.*, [2013], where they find that evapotranspiration intensified the summer drought in these catchments.

In another example, the case of mean annual runoff in Fig. 7a (case of combined climate and land use change), we find that for increases in mean annual precipitation greater than 25%, the likelihood of the mean annual runoff belonging to extremely high values (Class C3) is greatest if the percentage of deep-rooted vegetation in the watershed is less than 36%. If the percentage of vegetation is greater than 36%, depending on particular climate and temperature changes, the indicator values may fall in the historically observed ranges or be slightly higher than historically observed values (Class C1 or C2).

5 Conclusions

In this study, we develop a vulnerability-based approach to quantify the impact of climate and land use change on several streamflow indicators while considering hydrologic model parameter uncertainty. We explore a large space of climates, land uses and hydrologic model parameters, in order to understand their relative control on selected streamflow indicators, and find that different controls emerge across indicators. We also find that the sensitivity of streamflow to temperature and precipitation change depends upon the magnitude of the precipitation change itself. For example, the values of mean annual runoff are relatively insensitive to temperature change if mean annual precipitation decreases beyond -35% of the historical value. The classification trees produced demonstrate that climate, soils, vegetation and geomorphology (recession) come together in a complex manner to generate different streamflow regimes and characteristics. For each indicator, the different branches of the tree represent different states for the watershed resulting from combinations of climate and physical characteristics.

There are three possible ways in which the bottom up approach can assist the decision maker. Firstly, the detection of dominant controls on a hydrologic indicator helps the stakeholder to assess where investments should be made to attempt to reduce uncertainties. For example, it is clear from the classification tree of mean annual runoff that the reduction in uncertainty associated with future precipitation is very important. Secondly, the values of adverse climate and land use thresholds provide the decision maker with an indication of how robust a watershed is to changing conditions. If small changes in climate/land use cause a transition to vulnerable regimes, a highly risk averse strategy should be followed to tackle such potential future change. Thirdly, studies focusing on impact of climate change on water resources generally neglect the role of land use change while both are likely to occur concurrently in watersheds. We provide one way to combine both of these stressors in a common framework.

There are limitations in this study that allow for future improvements. First of all, the exploration of climate space using the delta change method does not allow the stakeholder to analyze the impact of changing precipitation characteristics beyond the mean amount (e.g. frequency of wet days) on the resultant streamflow indicator. This limits our ability to test how precipitation changes will impact frequency characteristics of streamflow. Use of weather generators that allow the variation in several hydrologically relevant characteristics of precipitation could reduce this problem in the future. Also, the modeled impact of land use change in our study is based on percentage of vegetation in the watershed and does not consider the impact of changing leaf area indices on interception or other vegetation related hydrologic impacts.

We also show that the classification trees derived using this approach may show some dependence upon the choice of vulnerability thresholds for the hydrologic indicators. Furthermore, the results presented here are from as single model structure that leaves model structural uncertainty unaccounted for in our current analysis. However, the framework can potentially incorporate this uncertainty due to its ability to incorporate categorical data that allows for inclusion of more than one model structures as separate categories of input data. Finally, there can be large uncertainties (large misclassification error rates) in the classification trees themselves, indicating a complex control on the hydrologic indicator that is not easily segregated by using CART. While we have addressed this issue by representing this uncertainty visually as histograms at each leaf node, other classification methods (such as random forests) can be explored in the future for addressing such cases.

In summary, our method allows stakeholders to assess the vulnerability of a watershed to climate and land use change within a hydrologic modeling framework. It provides a novel way to incorporate various sources of information about the watershed's behavior to assess its response to changing climate or land use or both. By combining the results of this approach with available climate projections, decisions makers will be better equipped to appraise different alternatives for future action.

Acknowledgements

This research was supported by the Office of Science (BER), US Department of Energy, Grant No. DE-FG02-08ER64641 and an EPA STAR Early Career Grant RD834196. This work was partially supported by the Natural Environment Research Council (Consortium on Risk in the Environment: Diagnostics, Integration, Benchmarking, Learning and Elicitation (CREDIBLE); NE/J017450/1). All the data used in the paper has been obtained from free available sources cited in the manuscript.

References

Arnold, J. G., P.M. Allen, R. Muttiah, and G. Bernhardt (1995), Automated base flow separation and recession analysis techniques, *Ground Water*, 33(6), 1010–1018, doi: 10.1111/j.1746584.1995.tb00046.

Bai, Y., T. Wagener, and P. Reed (2009), A top-down framework for watershed model evaluation and selection under uncertainty, *Environ. Modell. Softw.*, doi:10.1016/j.envsoft.2008.12.012.

Barron, E.J. (2009), Beyond climate science, Science, 326, 643.

Bennett, K., A. Werner, and M. Schnorbus (2012), Uncertainties in Hydrologic and Climate Change Impact Analyses in Headwater Basins of British Columbia, *J. Climate*, doi:10.1175/JCLI-D-11-00417.1, in press.

Beven, K. (2011), I believe in climate change but how precautionary do we need to be in planning the future? *Hydrol. Process.*, 25, 1517-1520, doi: 10.1002/hyp.7939.

Boso, F., F.P.J. de Barros, A. Fiori, and A. Bellin (2013), Performance analysis of statistical spatial measures for contaminant plume characterization towards risk-based decision making, *Water Resour. Res.*, accepted article, doi: 10.1002/wrcr.20270.

Bosshard, T., M. Carambia, K. Goergen, S. Kotlarski, P. Krahe, M. Zappa, and C. Schäär (2013), Quantifying uncertainty sources in an ensemble of hydrological climate-impact Projections, *Water Resour. Res.*, 49, 1523-1536, doi:10.1029/2011WR011533.

Brazil, L.E. (1988), Multilevel calibration strategy for complex hydrologic simulation models, *PhD thesis*, Colorado State University, Fort Collins, Colorado.

Breiman, L., J.H. Friedman, R.A. Olshen, and C.J. Stone (1984), Classification and regression trees, CRC Press.

Brown, C., W. Werick, W. Leger, and D. Fay (2011), A Decision-Analytic Approach to Managing Climate Risks: Application to the Upper Great Lakes, *J. Am. Water Resour. As.*, 47(3), 524-534, doi: 10.1111/j.1752-1688.2011.00552.x.

Chen, J., F.P. Brissette, A. Poulin, and R. Leconte (2011), Overall uncertainty study of the hydrological impacts of climate change for a Canadian watershed, *Water Resour. Res.*, 47, W12509, doi: 10.1029/2011WR010602.

Christensen, J.H., B. Hewitson, A. Busuioc, A. Chen, X. Gao, I. Held, R. Jones, R.K. Kolli, W.-T. Kwon, R. Laprise, V. Magaña Rueda, L. Mearns, C.G. Menéndez, J. Räisänen, A. Rinke, A. Sarr, and P. Whetton (2007), Regional Climate Projections, in Climate Change 2007: The Physical Science Basis. Contribution of Working Group I to the Fourth Assessment Report of the Intergovernmental Panel on Climate Change edited by S. Solomon, et al., Cambrige, UK, and New York, USA: Cambridge University Press.

Collins, M., R.E., Chandler, P.M. Cox, J.M. Huthnance, J. Rougier, and D.B. Stephenson (2012), Quantifying future climate change, *Nat. Clim. Chang.*, 2, 403-409, doi:10.1038/nclimate1414.

Dobler, C., S. Hagemann, R.L. Wilby, and J. Stötter (2012), Quantifying different sources of uncertainty in hydrological projections at the catchment scale, *Hydrol. Earth Syst. Sci. Discuss.*, 9, 8173-8211, doi: 10.5194/hessd-9-8173-2012.

Duan, Q., J. Schaake, V. Andreassian, S. Franks, H.V. Gupta, Y.M. Gusev, F. Habets, A. Hall, L. Hay, T.S. Hogue, M. Huang, G. Leavesley, X. Liang, O.N. Nasonova, J. Noilhan, L. Oudin, S. Sorooshian, T. Wagener, and E.F. Wood (2006), The Model Parameter Estimation Experiment (MOPEX): An overview of science strategy and major results from the second 20 and third workshops, *J. Hydrol.*, 320(1–2), 3–17, doi:10.1016/j.jhydrol. 2005.07.031.

Falcone, J. A., D.M. Carlisle, D.M. Wolock, and M.R. Meador (2010), GAGES: A stream gage database for evaluating natural and altered flow conditions in the conterminous United States, *Ecology*, 91:621.

Farmer, D., M. Sivapalan, and C. Jothityangkoon (2003), Climate, soil, and vegetation controls upon the variability of water balance in temperate and semiarid landscapes: Downward approach to water balance analysis, *Water Resour. Res.*, 39(2), 1035.

Frans, C., E. Istanbulluoglu, V. Mishra, F. Munoz-Arriola, and D.P. Lettenmaier (2013), Are climatic or land cover changes the dominant cause of runoff trends in the Upper Mississippi River Basin? *Geophys. Res. Lett.*, 40, 1104–1110, doi:10.1002/grl.50262.

Hall, J. (2007), Probabilistic climate scenarios may misrepresent uncertainty and lead to bad adaptation decisions, *Hydrol. Process.*, 21, 1127–1129, doi:10.1002/hyp.6573.

Hargreaves, G.H., and Z.A. Samani (1985), Reference crop evapo-transpoiration from temperature, *Appl. Eng. Agric.*, 1(2), 96:99.

Jones, R.N., H.S.C. Francis, W.C. Boughton, and L. Zhang (2006), Estimating sensitivity of mean annual runoff to climate change using selected hydrologic models, *Adv. Water Resour.*, 29, 1419-1429, doi: 10.1016/j.advwatres.2005.11.001.

Kapangaziwiri, E., D.A. Hughes, and T. Wagener (2012), Incorporating uncertainty in hydrological predictions for gauged and ungauged basins in southern Africa, *Hydrol. Sci. J.*, 57 (5), 1000-1019.

Kay, A.L., H.N. Davies, V.A. Bell, and R.G. Jones (2009), Comparison of uncertainty sources for climate change impacts: flood frequency in England, *Clim. Chang.*, 92(1–2), 41–63, doi: 10.1007/s10584-008-9471-4.

Khader, A.I., D.E. Rosenberg, and M. McKee (2013), A decision tree model to estimate the value of information provided by a groundwater quality monitoring network, *Hydrol. Earth. Syst. Sci.*, 17, 1797-1807, doi: 10.5194/hess-17-1979-2013.

Knutti, R., D. Masson, and A. Gettelman (2013), Climate model genealogy: Generation CMIP5 and how we got there, *Geophys. Res. Lett.*, 40, 1194–1199, doi:10.1002/grl.50256.

Kollat, J.B., P.M. Reed, and T. Wagener (2013) When are multiobjective calibration tradeoffs in hydrologic models meaningful? *Water Resour. Res.*, 48, W03520, doi: 10.1029/2011WR011534.

Kottegoda, N.T., and R. Rosso (1997), Statistics, probability and reliability for Civil and Environmental Engineers, McGraw-Hill, U.S.A.

Kunreuther, H., G. Heal, M. Allen, O. Edenhofer, C.B. Field, and G. Yohe (2013), Risk management and climate change, *Nat. Clim. Chang.*, 3, 447-450, doi: 10.1038/NCLIMATE1740.

Lempert, R.J., B.P. Bryant, and S.C. Bankes (2008), Comparing algorithms for scenario discovery, Working Paper, WR-557-NSF, RAND Corporation, Santa Monica, California.

Manning, L. J., J.W. Hall, H.J. Fowler, C.G. Kilsby, and C. Tebaldi (2009), Using probabilistic climate change information from a multimodel ensemble for water resources assessment, *Water Resour. Res.*, 45, W11411, doi:10.1029/2007WR006674.

Maurer, E. P., and P.B. Duffy (2005), Uncertainty in projections of streamflow changes due to climate change in California, *Geophys. Res. Lett.*, 32, L03704, doi:10.1029/2004GL021462.

Merz, R., J. Parajka, and G. Blöschl (2010), Time stability of catchment model parameters: Implications for climate impact analyses, *Water Resour. Res.*, 47, W02531, doi: 10.1029/2010WR009505.

Milly, P.C.D., R.T. Wetherald, K.A. Dunne, and T.L. Delworth (2002), Increasing risk of great floods in a changing climate, *Nature*, 415, 514-517.

Moody, P., and C. Brown (2013), Robustness indicators for evaluation under climate change: application to the Upper Great Lakes, *Water Resour. Res.*, accepted article, doi: 10.1002/wrcr.20228.

Nash, J. E., and J.V. Sutcliffe (1970), River flow forecasting through conceptual models part I — A discussion of principles, *J. of Hydrol.*, 10 (3), 282–290.

Nash, L.L., and P.H. Gleick (1991), Sensitivity of streamflow in the Colorado basin to climatic changes, *J. of Hydrol.*, 125, 221-241, doi: 10.1016/0022-1694(91)90030-L.

Ning, L., M.E. Mann, R. Crane, and T. Wagener (2012a), Probabilistic Projections of Climate Change for the Mid-Atlantic Region of the United States: Validation of Precipitation Downscaling during the Historical Era, *J. Climate*, 25, 509-526, doi: 10.1175/2011JCLI4091.1.

Ning, L., M.E. Mann, R. Crane, T. Wagener, R.G. Najjar Jr., and R. Singh (2012b), Probabilistic Projections of Climate Change Impacts on Precipitaiton for the Mid-Atlantic Region of the United States, *J. Climate*, 25, 509-526, doi: 10.1175/2011JCLI4091.1.

Olden, J.D., and N.L. Poff (2003), Redundancy and the choice of hydrologic indices for characterizing streamflow regimes, *River Res. Appl.*, 19, 101-121.

Paton, F. L., H.R. Maier, and G.C. Dandy (2013), Relative magnitudes of sources of uncertainty in assessing climate change impacts on water supply security for the southern Adelaide water supply system, *Water Resour. Res.*, 49, 1643–1667, doi:10.1002/ wrcr.20153.

Prudhomme, C., and H. Davies (2009a), Assessing uncertainties in climate change impact analyses on the river flow regimes in the UK. Part 1: baseline climate, *Clim. Chang.*, 93: 177–195, doi: 10.1007/s10584-008-9464-3.

Prudhomme, C., and H. Davies (2009b), Assessing uncertainties in climate change impact analyses on the river flow regimes in the UK. Part 2: future climate, *Clim. Chang.*, 93: 197–222, doi: 10.1007/s10584-008-9461-6.

Sawicz, K., 2013. Catchment classification – understanding hydrologic similarity through catchment function. *PhD Thesis*, The Pennsylvania State University, University Park, PA.

Son, K., and M. Sivapalan (2007), Improving model structure and reducing parameter uncertainty in conceptual water balance models through the use of auxiliary data, *Water Resour. Res.*, 43, W01415, doi:10.1029/2006WR005032.

Singh, R., T. Wagener, K. van Werkhoven, M.E. Mann, and R. Crane (2011), A trading-space-for-time approach to probabilistic continuous streamflow predictions in a changing climate – accounting for changing watershed behavior, *Hydrol. Earth Syst. Sci.*, 15, 3591-3603, doi: 10.5194/hess-13591-2011.

Singh, R., K. van Werkhoven, and T. Wagener (2013), Hydrologic impacts of climate change in gaugaed and ungauged watersheds of the Olifants Basin - A trading space-for-time approach, *Hydrol. Sci. J.*, 59 (1), 29-55, doi: 10.1080/02626667.2013.819431.

Stephenson, D.B., M. Collins, J.C. Rougier, and R.E. Chandler (2012), Statistical problems in the probabilistic prediction of climate change, *Environmetrics*, 23 (5), 364-372, doi: 10.1002/env.2153.

Teng, J., J. Vaze, F.H.S. Chiew, B. Wang, and J.-M. Perraud (2012), Estimating the Relative Uncertainties Sourced from GCMs and Hydrological Models in Modeling Climate Change Impact on Runoff, *J. Hydrometeorol.*, 13, 122–139, doi: http://dx.doi.org/10.1175/JHM-D-11-058.1.

Teuling, A. J., A.F. Van Loon, S.I. Seneviratne, I. Lehner, M. Aubinet, B. Heinesch, C. Bernhofer, T. Grünwald, H. Prasse, and U. Spank (2013), Evapotranspiration amplifies European summer drought, *Geophys. Res. Lett.*, 40, doi:10.1002/grl.50495.

Therneau, T.M., and E.J. Atkinson (1997), An introduction to recursive partitioning using the RPART routines, Technical Report 61, Mayo Clinic, Section of Statistics. Accessed online on 24th January 2014 from: http://www.mayo.edu/hsr/techrpt/61.pdf

Van Werkhoven, K., T. Wagener, P. Reed, and Y. Tang (2008), Characterization of watershed model behavior across a hydroclimatic gradient, *Water Resour. Res.,* 44, W01429, doi:10.1029/2007WR006271.

Wagener, T., M. Sivapalan, P.A. Troch, B.L. McGlynn, C.J. Harman, H.V. Gupta, P. Kumar, P.S.C. Rao, N.B. Basu, and J.S. Wilson (2010), The future of hydrology: an evolving science for a changing world, *Water Resour. Res.*, 46, W05301, doi: 10.1029/2009WR008906

Weaver, C.P., R.J. Lempert, C. Brown, J.A. Hall, D. Revell, and D. Sarewtiz (2013), Improving the contribution of climate model information to decision making: the value and demands of robust decision frameworks, *WIREs Clim. Change.,* 4, 39-60, doi: 10.1002/wcc.202.

Wilby, R. L., and I. Harris (2006), A framework for assessing uncertainties in climate change impacts: Low-flow scenarios for the River Thames, UK, *Water Resour. Res.*, 42, W02419, doi:10.1029/2005WR004065.

Wilby, R.L., and S. Dessai (2010), Robust adaptation to climate change, Weather, 65(7), 180-185, doi: 10.1002/wea.543.

Xu, C.-y., E. Wildén, and S. Halldin (2005), Modelling Hydrological Consequences of Climate Change – Progress and Challenges, *Adv. Atmos. Sci.*, 22 (6), 789-797, doi: 10.1007/BF02918679.

Zhao, R.J., Y.L. Zhang, L.R. Fang, X.R. Liu, and Q.S. Zhang (1980), The Xinanjiang model, in, *Hydrological Forecasting*, IASH Publ., 129, 351-356.

List of Tables

Table 1 Definition of hydrologic indicators analyzed in the study based on *Olden and Poff* [2003].

Table 2 Feasible and a-priori ranges of the hydrologic model parameters.

Table 3 List of general circulation models (GCMs) that are used for statistically downscaling the precipitation and temperature data. The data is downscaled for baseline (1961-2000) and end of century (2081-2100) for A2 emission scenario.

List of Figures

Figure 1 (a) The hydro-climatic framework showing the traditional forward propagation approach used to derive future changes in hydrologic variables of interest (b) The bottom-up approach used in this study, which starts by defining different (slightly vulnerable/vulnerable/ non-vulnerable etc.) classes for a hydrologic indictor of interest and then identifying the regions in the input space that lead to each class.

Figure 2 The exploratory modelling framework used in this study. We explore a space spanned by NxP climate and hydrologic model parameter combinations. For this study, N is a combination of 11 precipitation changes ranging from -50% to +50% in increments of 10% and 9 temperature changes ranging from +0°C to +8°C, resulting in 99 climates spanning the range of dry/hot to wet/cold climates. Number of parameter sets, P is fixed at 10000 randomly generated sets of hydrologic model parameters. Therefore, in total, for each hydrologic indicator, we explored a combined space of 990,000 points. We use classification and regression trees (CART) to relate the resultant streamflow indicators from the NxP climate-parameter combinations to the classes defined on the right hand side.

Figure 3 Top down model structure used in the study. The model has representations for snow and vegetation. The soil depth is modelled as a probability distribution of 10 buckets reflecting variable soil depths.

Figure 4 Study area: The Lower Juniata watershed and the location of the streamflow gauge.

Figure 5 Method for defining the different classes for hydrologic indicator values. Example is shown for low flow pulse duration. First a 10-year running window from 1948-2002 is used to obtain 45 values for each period. The range across these values is used to derive the mean and standard deviation for the indicator values. Then the classes are defined based on the mean and standard deviation estimates as explained in the text.

Figure 6 (a) Class assignment for flood frequency indicator. The grey markers represent the historically observed values of the indicator. W is the width of the classes. (b) Classification tree for flood frequency for class width of 4 S.D, and (c) 6 S.D. Class probabilities associated with classes 1 to 7 are represented by vertical bars at each node of the tree. Solid black lines represent the paths to vulnerability. Classes C2, C3 and C6 represent classes for increased values of high flood frequency, and are assumed to be vulnerable. Pratio is the ratio of future mean annual precipitation to the historical mean annual precipitation, so a value greater than 1 show an increase in mean annual precipitation and vice versa. ΔT is the increase in mean annual temperature in the future period from the historical period. Sb is the maximum height of soil moisture bucket and Ass is the recession coefficient from the saturated subsurface soil reservoir.

Figure 7 Combined impact of land use and climate change in the watershed for (a) Mean annual runoff and (b) maximum August flow. For both cases, there is only 1 path that can lead to the historically observed indicator range based on historical climate and land use, highlighted by black lines in each tree. The left panel shows the case when fraction of deep-rooted vegetation is fixed within historical range (0.6 to 0.8) and only climate is varied. Here, the black line follows the combinations of precipitation, and temperature that represent the climate of the watershed in the historical period. The right panel shows the case of varying fraction of deep-rooted vegetation (0 to 1) and climate together. Here, the black line follows the combinations of precipitation, temperature, and deep-rooted vegetation cover that represent the climate and forest cover of the watershed in the historical period. Both decision trees show that deep-rooted vegetation cover is a critical control on the hydrologic indicator. Pratio is the ratio of future mean annual precipitation to the historical mean annual precipitation, so a value greater than 1 shows an increase and vice versa. ΔT is the difference between the future temperature and historical mean annual temperature. %Vg is the percentage of deep-rooted vegetation in the watershed. B and Sb, are hydrologic model parameters representing the soil moisture accounting module.

Figure 8 Dominant controls on hydrologic indicators across climate (precipitation and temperature), fraction of deep-rooted vegetation (%Veg), soil parameters and recession (routing) parameters for (a) Feasible parameter range (b) a priori parameter range with fraction of deep rooting vegetation in historical range (0.6-0.8) and (c) a priori parameter range with fraction of deep-rooted vegetation varying between 0 and 1.

Figure 9 (a) CART result for flood frequency with class width (W) set at 4 standard deviations (b) Representing parametric uncertainty based on historical streamflow data using top 19 parameter sets satisfying NSE>0.75 and bias error <10%. The diamonds represent the cutoff value chosen by the classification tree for the indicator in (a). Feasible parameter values falling above and below A/B imply that there is uncertainty in deciding the terminal node to which the indicator belongs.

Figure 10 (a) Future ranges for precipitation and temperature change based on downscaled climate data. Precipitation change (Pratio) is expressed as the ratio of mean annual precipitation for end of century (2090-2100) projections to mean annual precipitation in the baseline (1990-2000) period. Temperature change (ΔT) is expressed as the difference between mean annual temperatures for end of century (2090-2100) projections to mean annual temperature in the baseline (1990-2000) period. (b) Classification tree for mean annual runoff. The black lines in (b) represent the future classes for mean annual streamflow derived from navigating the classification tree in (b) using precipitation and temperature changes in (a). (c) Projections of streamflow obtained by the traditional top-down approach by driving the hydrologic model directly with the future precipitation and temperature time series. 19 parameter sets fixed at their historically calibrated values are used. We compare the projections of mean annual streamflow derived from the bottom-up CART analysis in (b) to those derived directly from the top-down method using statistically downscaled GCM output (c).

Figure 11 Visualizing 200 randomly selected parameters and climate combinations that lead to Classes 1-5 for mean annual runoff. The horizontal bar plots on each subplot is the histogram for that particular parameter/climate variable. We find that precipitation and temperature changes mainly control the mean annual runoff. Fraction of deep-rooted vegetation (%Veg) is fixed at the historical values in this plot, therefore does not emerge as an important influence. ΔT and ΔP are mean annual precipitation and temperature changes. Ddf to Abf are the hydrologic model parameters whose ranges are fixed at the a-priori range.

Hydrologic Indicator	Category	Definition	Units
Mean annual runoff	Magnitude	Mean annual flow (normalized by catchment area)	mm/year
Minimum April flow	Magnitude-high	Mean minimum monthly flow for April across time period of study	mm/day
Maximum August flow	Magnitude-low	Mean maximum monthly flow for August across time period of study	mm/day
Low flow pulse count	Frequency – low	Number of annual occurrences during which the magnitude of flow remains below a lower threshold. Hydrologic pulses are defined as those periods within a year in which the flow drops below 25th percentile of all daily values for the time period	[-]
Flood frequency	Frequency – high	Same as above where high pulse is defined as 3 times the median daily flow	[-]
Low flow pulse duration	Duration – low	Mean duration of low flow pulses defined above	[days]
High flow pulse duration	Duration – high	Mean duration of high flow pulses with high flow cutoff at 75th percentile of the daily flows of the entire record	[days]
Seasonal predictability of non-flooding	Timing of change	Maximum proportion the year (number of days/365) during which no floods have ever occurred over the period of record. Floods are defined as flow values greater than or equal to flows with 60% exceedance probability (1.67 year return interval)	[-]
Reversals	Rate of change	Number of negative and positive changes in water conditions from one day to the next	[-]

		Description	Feasible range		Reduced a-priori range[d]		UNITS
			Lower	Upper	Lower	Upper	
Soil	Sb	Max height of soil store	0	2000[a]	290	810	[mm]
	B	Distribution of buckets	0	7[a]			[-]
	FC	Field capacity parameter	0	1	0.24	0.96	[-]
	Kd		0	0.5[c]			[-]
Vegetation	%Veg	Deep-rooted vegation	0	1	0.6	0.8	[-]
	LAImax	Maximum leaf area index	0	6	0	6	[mm]
	LAImin	Minimum leaf area index	0	6	0	6	[mm]
Routing	ASS	Recession coefficient for saturated soil	1	20[b]	6	14	[days^{-1}]
	ABF	Recession coefficient for ground water	20	200[b]	50	83	[days^{-1}]
Snow	Ddf	Degree day factor	0	20[a]			[mm °C^{-1} d^{-1}]
	Tth	Threshold temperature for snow formation	-5	5[a]			[°C]
	Tb	Base temperature for melt	-5	5[a]			[°C]

[a] Kollat et al., [2013]
[b] Van Werkhoven et al., [2008]
[c] Farmer et al., [2003]
[d] Appendix B and Section 3.1

No	Abbreviation	CMIP3 I.D.	Origination group	Country
1	CGCM3.1	CGCM3.1 (T47)	Canadian Centre for Climate Modelling and Analysis	Canada
2	CM3	CNRM-CM3	Météo-France/Centre National de Recherches Météorolgiques	France
3	MK3.0	CSIRO-MK3.0	CSIRO Atmospheric Research	Australia
4	CM2.0	GFDL-2.0	US Dept. of Commerce/ NOAA/Geophysical Fluid Dynamics Laboratory	USA
5	GISS	GISS-ER	NASA/ Goddard Institute for Space Studies	USA
6	CM4	IPSL-CM4	Institute Pierre Simon Laplace	France
7	ECHOG	ECHO-G	Meteorological Institute of the University of Bonn, Meteorological Research Institute of KMA, and Model and Data group	Germany Korea
8	ECHAM5	ECHAM5/MPI-OM	Max Planck Institute of Meteorology	Germany
9	CGCM2.3.2a	MRI-CGCM2.3.2a	Meteorological Research Institute	Japan

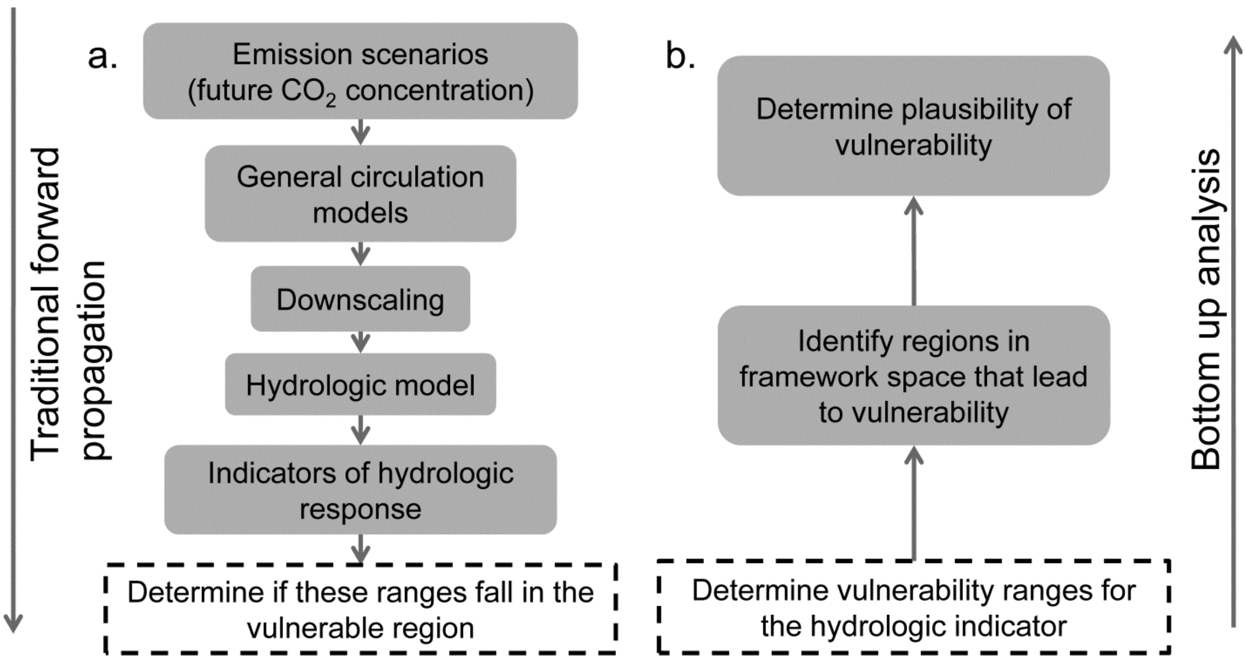

a.
Emission scenarios
(future CO_2 concentration)
General circulation models
Downscaling
Hydrologic model
Indicators of hydrologic response
Determine if these ranges fall in the vulnerable region
Traditional forward propagation
b.
Determine plausibility of vulnerability
Identify regions in framework space that lead to vulnerability
Determine vulnerability ranges for the hydrologic indicator
Bottom up analysis

Figure 1

929

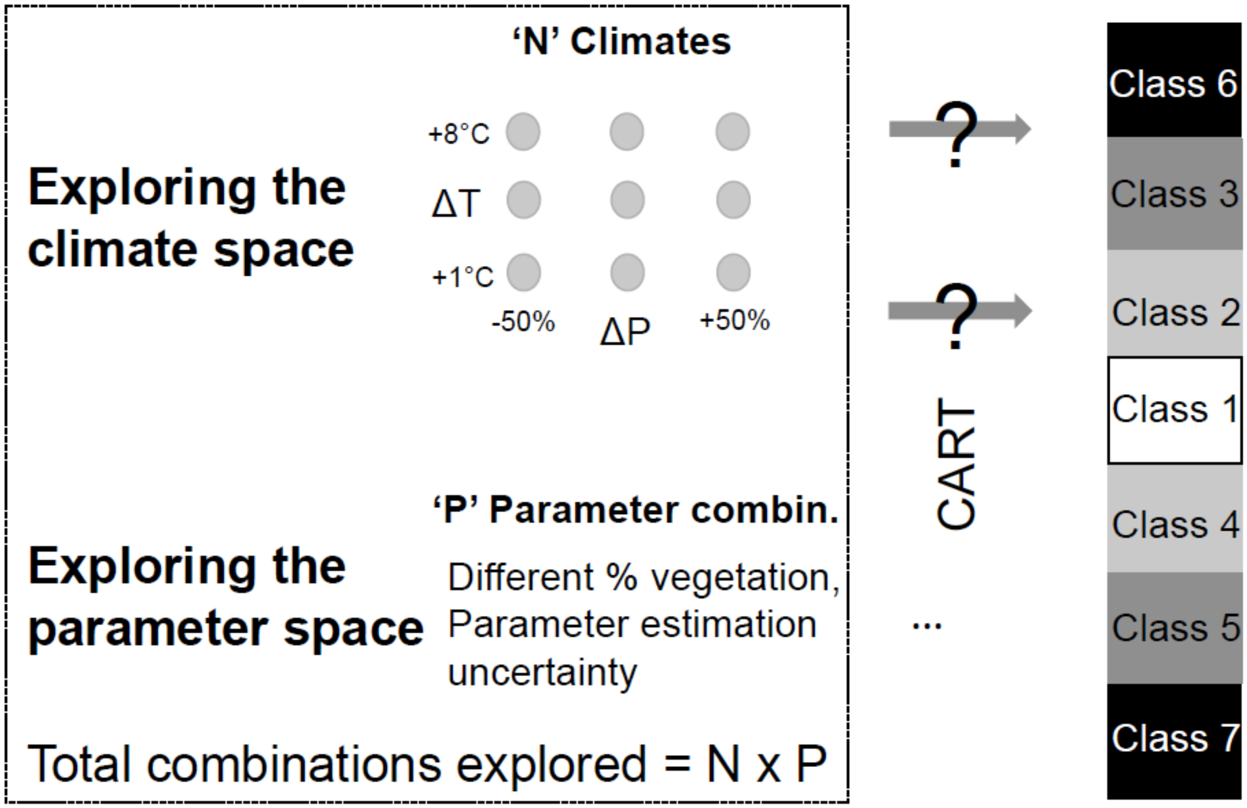
'N' Climates
Exploring the climate space
+8°C
ΔT
+1°C
-50%
ΔP
+50%
'P' Parameter combin.
Exploring the parameter space
Different % vegetation, Parameter estimation uncertainty
Total combinations explored = N x P
?
?
CART
...
Class 6
Class 3
Class 2
Class 1
Class 4
Class 5
Class 7

Figure 2

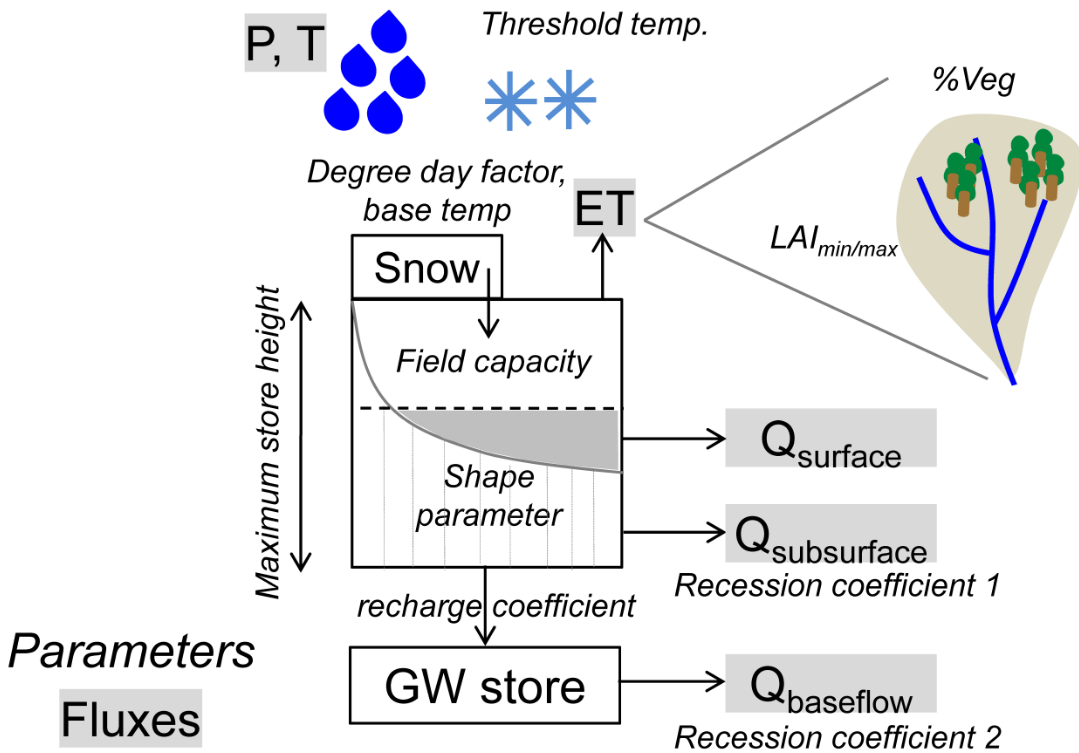

P, T
Threshold temp.
%Veg
Degree day factor,
base temp
ET
LAI$_{min/max}$
Snow
Field capacity
Maximum store height
Shape
parameter
Q$_{surface}$
Q$_{subsurface}$
Recession coefficient 1
recharge coefficient
Parameters
Fluxes
GW store
Q$_{baseflow}$
Recession coefficient 2

Figure 3

931

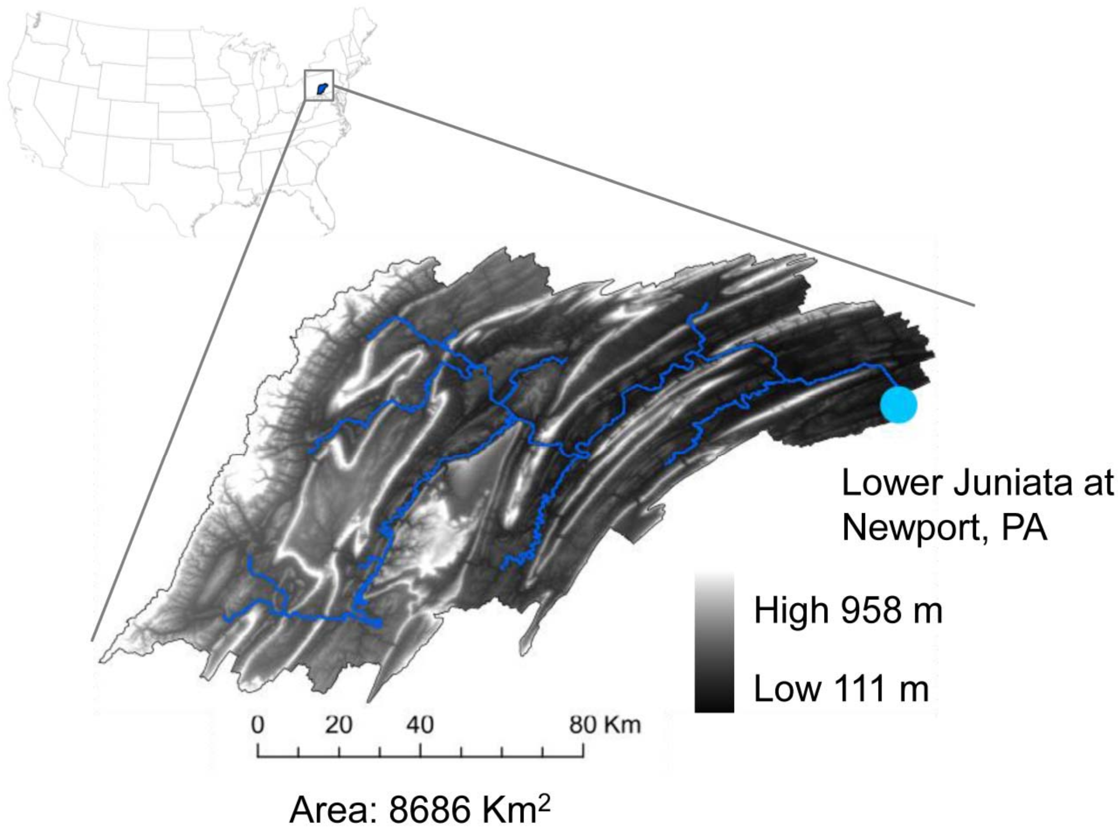
Lower Juniata at
Newport, PA
High 958 m
Low 111 m
0 20 40 80 Km
Area: 8686 Km2

Figure 4

933

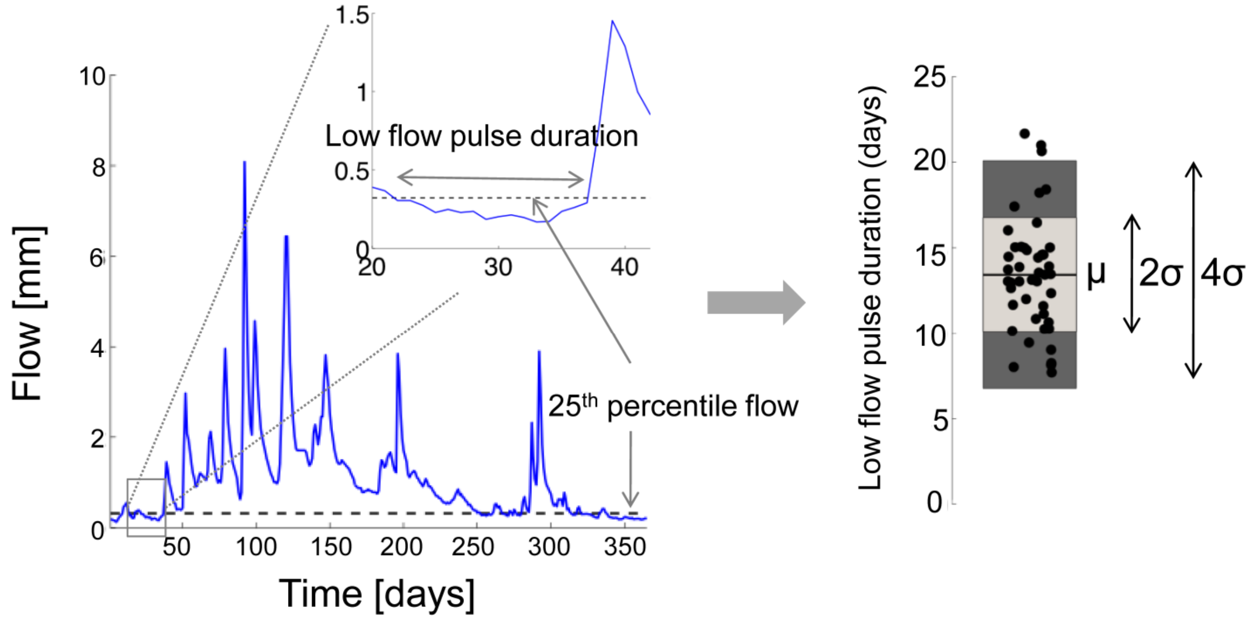

Flow [mm]
Time [days]
Low flow pulse duration
25th percentile flow
Low flow pulse duration (days)
μ
2σ
4σ

Figure 5

934

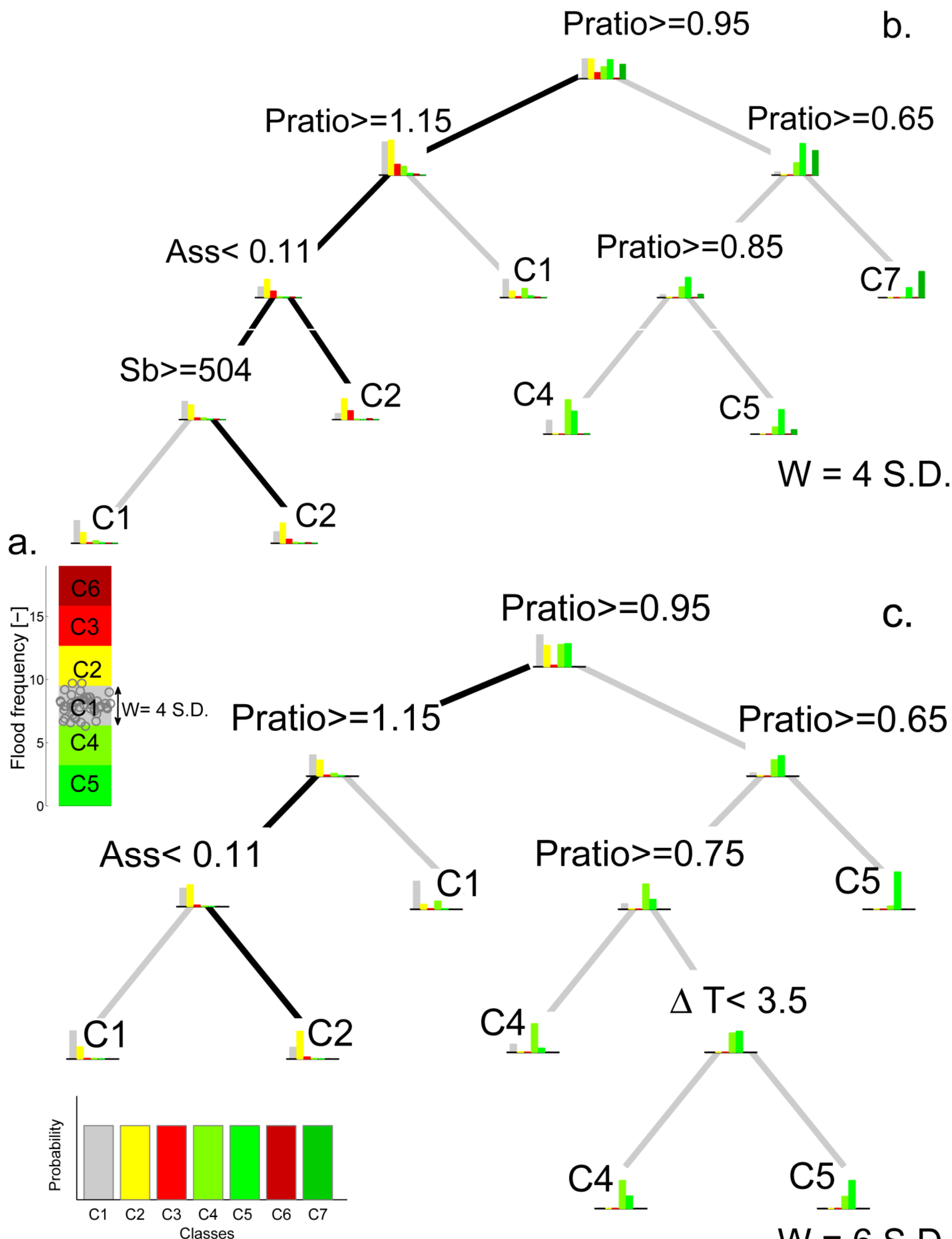

b.
Pratio>=0.95
Pratio>=1.15
Pratio>=0.65
Ass< 0.11
C1
Pratio>=0.85
C7
Sb>=504
C2
C4
C5
W = 4 S.D.
C1
C2
a.
C6
C3
C2
C1
C4
C5
W= 4 S.D.
Flood frequency [–]
0
5
10
15
c.
Pratio>=0.95
Pratio>=1.15
Pratio>=0.65
Ass< 0.11
C1
Pratio>=0.75
C5
C1
C2
C4
Δ T< 3.5
C4
C5
W = 6 S.D.
Probability
C1
C2
C3
C4
C5
C6
C7
Classes

Figure 6

935

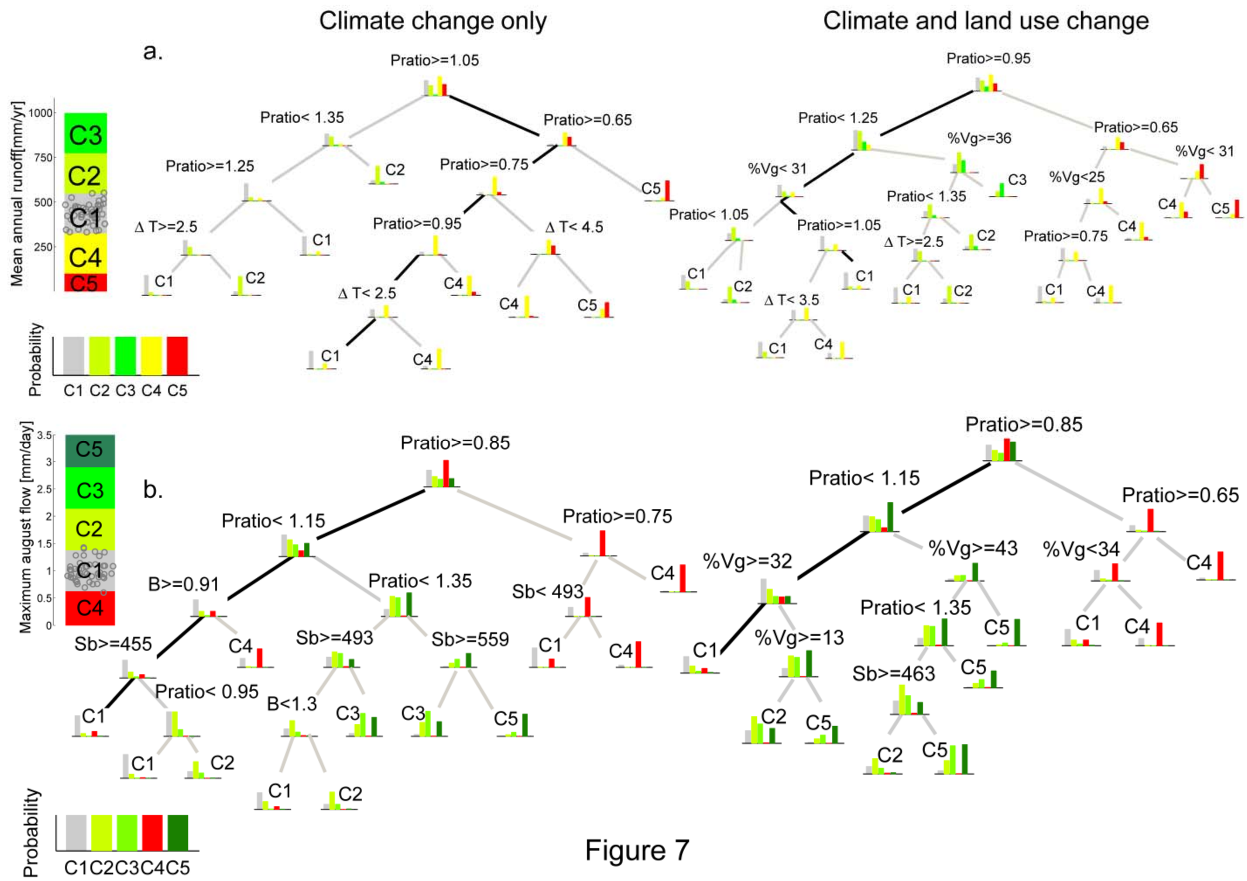
Climate change only
Climate and land use change
a.
b.
Mean annual runoff[mm/yr]
Maximum august flow [mm/day]
Probability
C1 C2 C3 C4 C5
Pratio>=1.05
Pratio< 1.35
Pratio>=0.65
Pratio>=1.25
Pratio>=0.75
Pratio>=0.95
Δ T>=2.5
Δ T< 4.5
Δ T< 2.5
Pratio>=0.95
Pratio< 1.25
Pratio>=0.65
%Vg>=36
%Vg< 31
%Vg<25
%Vg< 31
Pratio< 1.05
Pratio< 1.35
Pratio>=1.05
Δ T>=2.5
Pratio>=0.75
Δ T< 3.5
Pratio>=0.85
Pratio< 1.15
Pratio>=0.75
B>=0.91
Pratio< 1.35
Sb< 493
Sb>=455
Sb>=493
Sb>=559
Pratio< 0.95
B<1.3
Pratio>=0.85
Pratio< 1.15
Pratio>=0.65
%Vg>=32
%Vg>=43
%Vg<34
%Vg>=13
Pratio< 1.35
Sb>=463

Figure 7

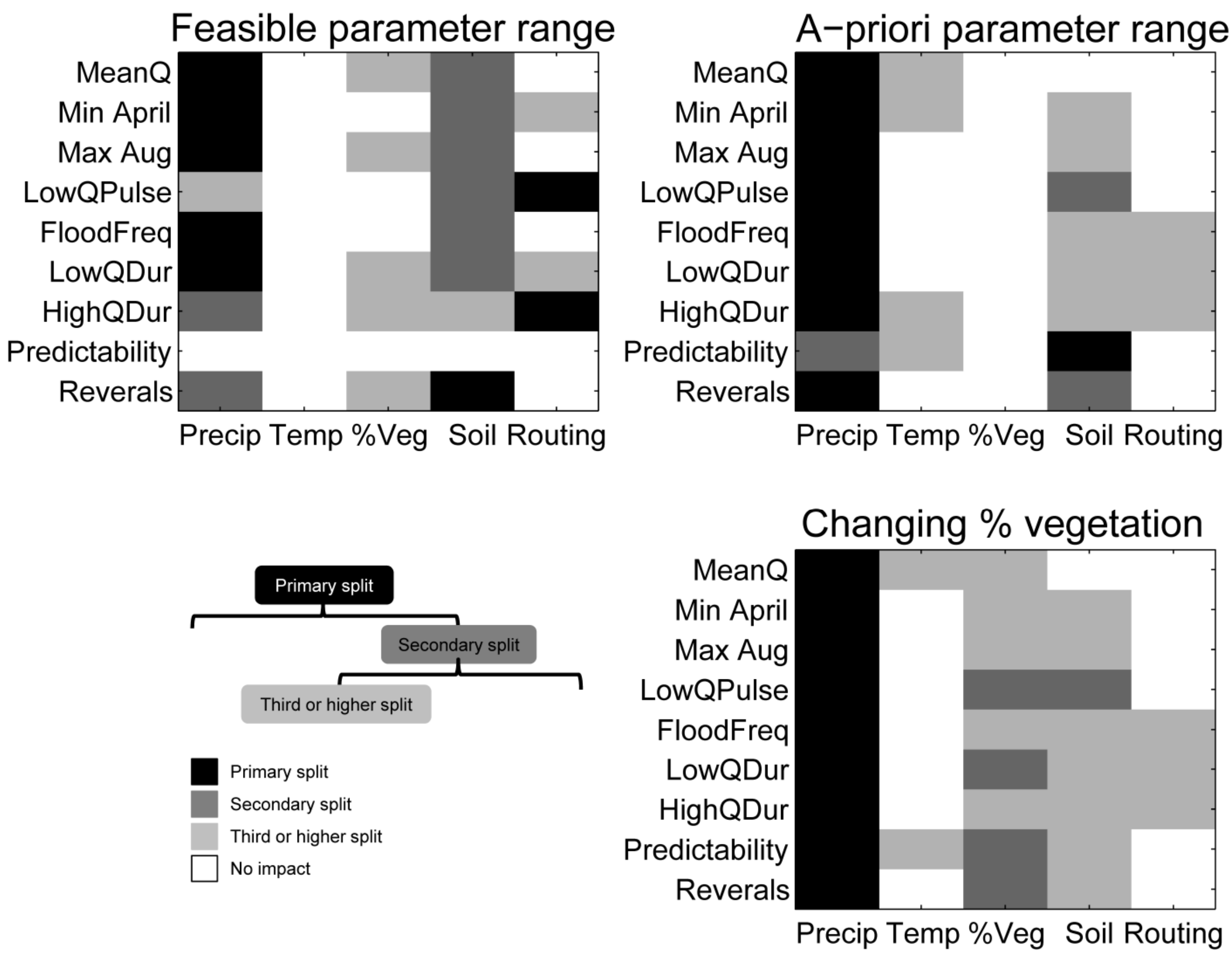
Feasible parameter range
A−priori parameter range
Changing % vegetation
MeanQ
Min April
Max Aug
LowQPulse
FloodFreq
LowQDur
HighQDur
Predictability
Reverals
Precip Temp %Veg Soil Routing
Primary split
Secondary split
Third or higher split
No impact

Figure 8

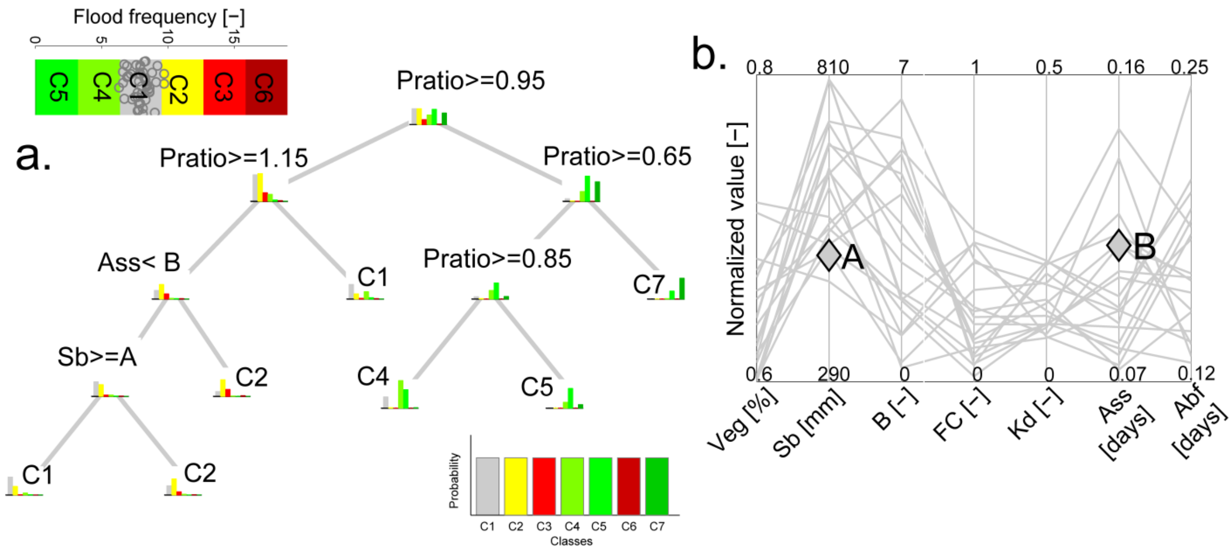
Flood frequency [−]
0
5
10
15
C5
C4
C1
C2
C3
C6
a.
Pratio>=0.95
Pratio>=1.15
Pratio>=0.65
Ass< B
C1
Pratio>=0.85
C7
Sb>=A
C2
C4
C5
C1
C2
Probability
C1 C2 C3 C4 C5 C6 C7
Classes
b.
Normalized value [−]
0.8 810 7 1 0.5 0.16 0.25
A
B
0.6 290 0 0 0 0.07 0.12
Veg [%]
Sb [mm]
B [−]
FC [−]
Kd [−]
Ass [days]
Abf [days]

Figure 9

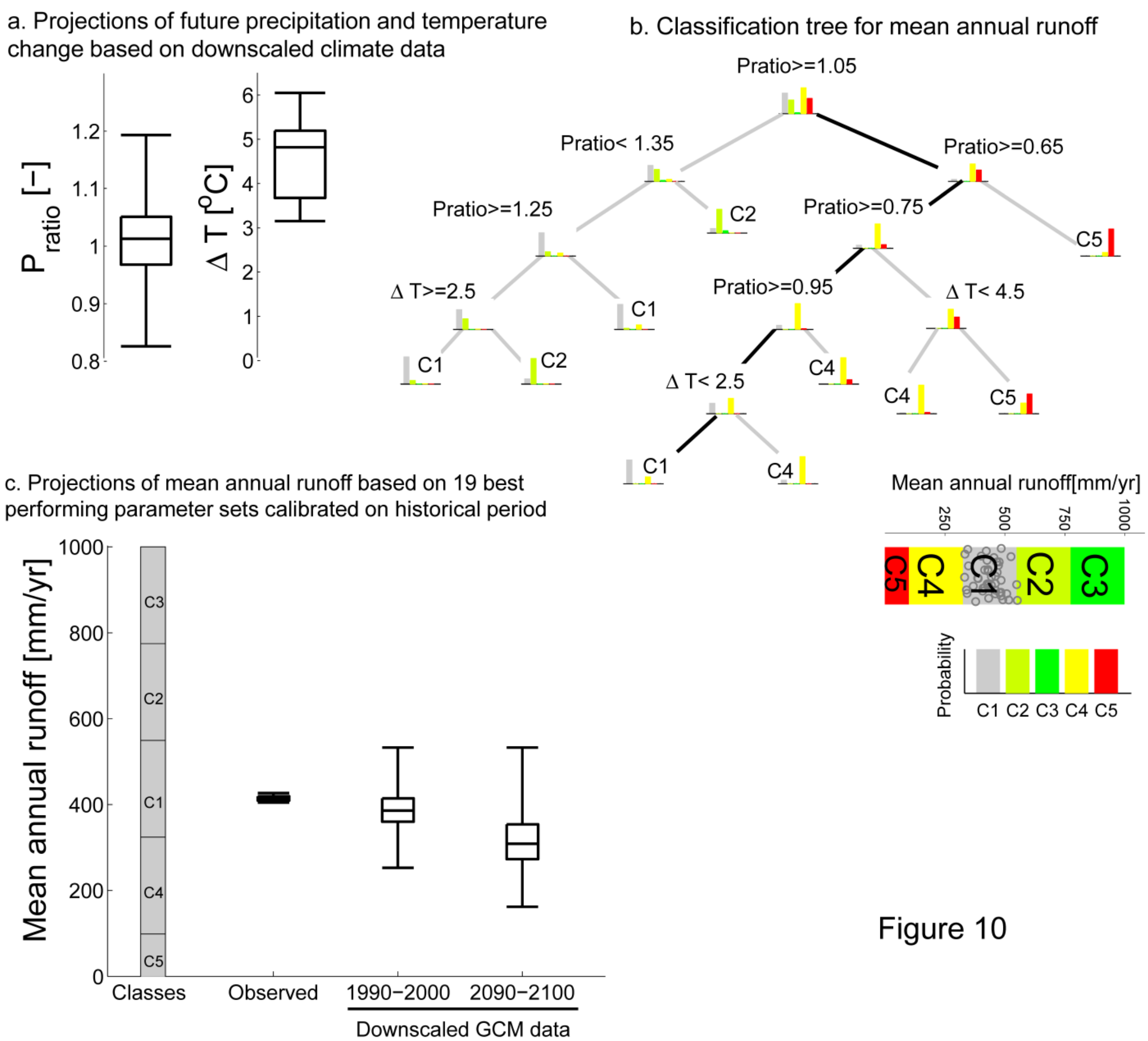

a. Projections of future precipitation and temperature change based on downscaled climate data
P ratio [-]
Δ T [°C]
b. Classification tree for mean annual runoff
Pratio>=1.05
Pratio< 1.35
Pratio>=0.65
Pratio>=1.25
C2
Pratio>=0.75
C5
Δ T>=2.5
C1
Pratio>=0.95
Δ T< 4.5
C1
C2
C4
Δ T< 2.5
C4
C5
C1
C4
Mean annual runoff[mm/yr]
250
500
750
1000
C5
C4
C1
C2
C3
Probability
C1 C2 C3 C4 C5
c. Projections of mean annual runoff based on 19 best performing parameter sets calibrated on historical period
Mean annual runoff [mm/yr]
Classes
Observed
1990−2000
2090−2100
Downscaled GCM data

Figure 10

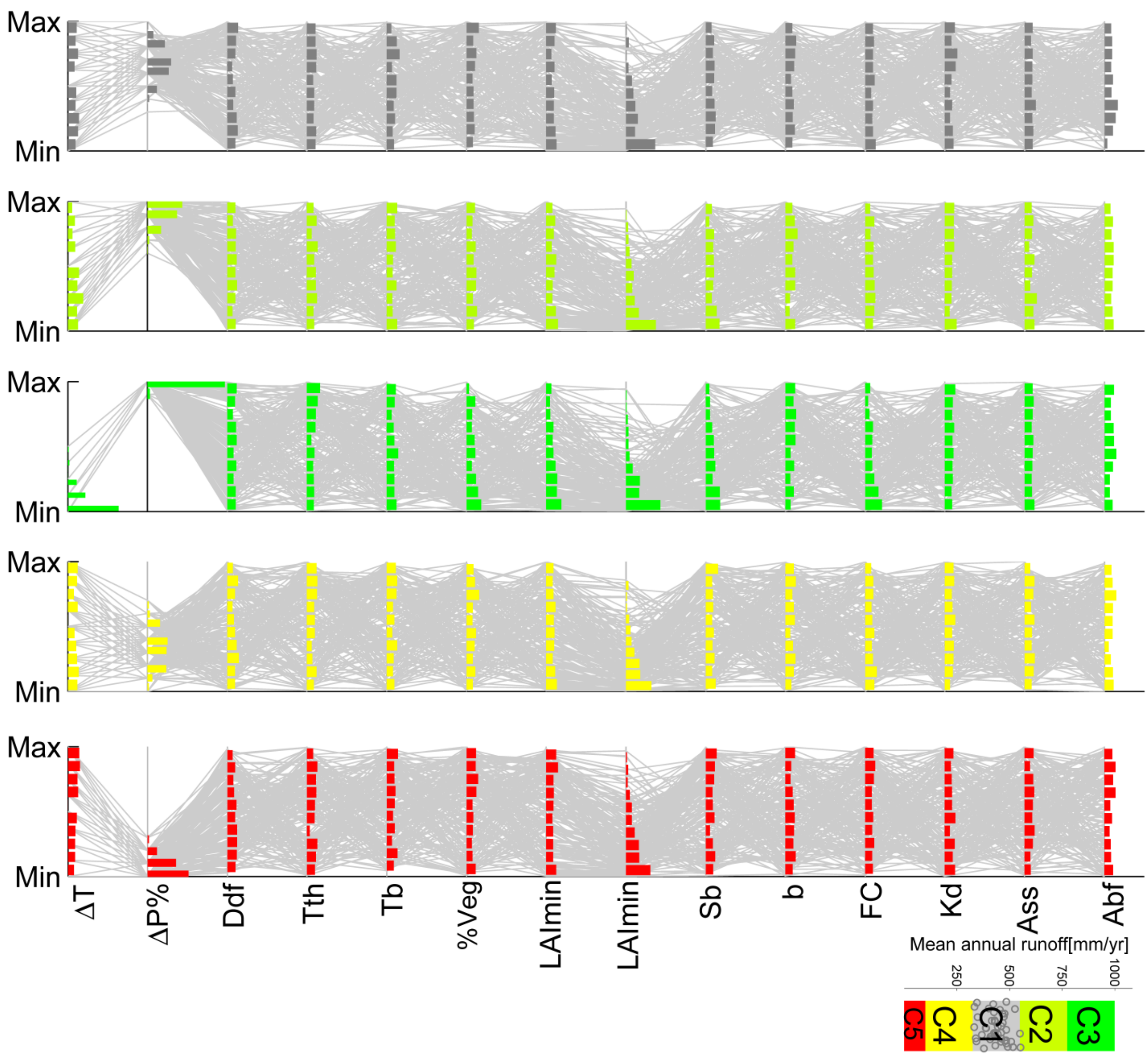

939 Figure 11